RSC Advances

PAPER

View Article Online
View Journal | View Issue

Open Access Article. Published on 07 October 2024. Downloaded on 2/11/2026 10:58:08 AM.
This article is licensed under a Creative Commons Attribution-NonCommercial 3.0 Unported Licence.

Check for updates

Cite this: *RSC Adv.*, 2024, **14**, 31607

Design, synthesis and *in vitro* anti-proliferative evaluation of new pyridine-2,3-dihydrothiazole/thiazolidin-4-one hybrids as dual CDK2/GSK3β kinase inhibitors†

Asmaa F. Kassem,[a] Ashraf A. Sediek,[b] Mervat M. Omran,[c] Doaa S. Foda[d] and Aisha A. K. Al-Ashmawy *[d]

Herein, the molecular hybridization drug discovery approach was used in the design and synthesis of twelve novel pyridine-2,3-dihydrothiazole hybrids (**2a,b–5a,b** and **13a,b–14a,b**) and fourteen pyridine-thiazolidin-4-one hybrids (**6a,b–12a,b**) as anti-proliferative analogues targeting CDK2 and GSK3β kinase inhibition. Almost all of the newly synthesized hybrids, including their precursors (**1a,b**), were evaluated for their anti-proliferative activity against three human cancer cell lines—MCF-7, HepG2 and HEp-2—as well as normal Vero cell lines. Both compounds **1a** (pyridine-thiourea precursor) and **8a** (pyridine-5-acetyl-thiazolidin-4-one hybrid) exhibited excellent anti-proliferative activity against HEp-2 (IC_{50} = 7.5 μg mL^{-1}, 5.9 μg mL^{-1}, respectively). Additionally, **13a** (pyridine-5-(*p*-tolyldiazenyl-2,3-dihydrothiazole)) hybrid demonstrated excellent anti-proliferative activity against HepG2 (IC_{50} = 9.5 μg mL^{-1}), with an acceptable safety profile against Vero (<45% inhibition at 100 μg mL^{-1}) in the cases of **8a** and **13a** alone. The three promising anti-proliferative hybrids (**1a**, **8a**, **13a**) were selected for the assessment of their *in vitro* inhibitory kinase activity against CDK2/GSK3β using roscovitine (IC_{50} = 0.88 μg mL^{-1}) and CHIR-99021 (IC_{50} = 0.07 μg mL^{-1}) as references, respectively. Compound **13a** was the most potent dual CDK2/GSK3β inhibitor (IC_{50} = 0.396 μg mL^{-1}, 0.118 μg mL^{-1}, respectively) followed by **8a** (IC_{50} = 0.675 μg mL^{-1}, 0.134 μg mL^{-1}, respectively), and the weakest was **1a**. To elucidate the mechanism of the most potent anti-proliferative **13a** hybrid, further cell cycle analysis was performed revealing that it caused G1 cell cycle arrest and induced apoptosis. Moreover, it resulted in an increase in Bax and caspase-3 with a decrease in Bcl-2 levels in HepG2 cells compared with untreated cells. Finally, *in silico* drug likeness/ADME prediction for the three potent compounds as well as a molecular docking simulation study were conducted in order to explore the binding affinity and interactions in the binding site of each enzyme, which inspired their usage as anti-proliferative leads for further modification.

Received 24th August 2024
Accepted 17th September 2024

DOI: 10.1039/d4ra06146b

rsc.li/rsc-advances

1 Introduction

Cancer is considered as the second largest cause of death and has been redefined as a broad category of various diseases.[1] According to a recent report of the International Agency for Research on Cancer (IARC), there were 10 million deaths and 19.5 million new cancer cases in 2020, and within 4 years, cancer is projected to become the first cause of death.[2] In conventional cancer treatments, including chemotherapy, radiotherapy and surgery, normal cells are observed to be badly affected, which is a major concern. Additionally, the development of multi-drug resistance to common chemotherapy presents a major challenge. All of these challenges prompted healthcare providers to use targeted therapies as a safer choice.[3] Protein kinase inhibitors (PKIs) provide the most attractive targeted oncotherapy in clinical use and the development of new cancer therapeutics, as they target the tumor cell microenvironment and signalling cascades with a minimal negative effect on normal cells.[4,5] Protein kinases, with 538 proteins, are classified into tyrosine, serine/threonine and dual-specificity kinases, as they catalyse the transfer of the terminal phosphate in ATP to the target protein.[6] This regulates and propagates the growth cell signal followed by differentiation, proliferation and apoptosis.[6] Any disturbance in PK regulation

[a]*Chemistry of Natural and Microbial Products Department, National Research Centre, Dokki, 12622, Cairo, Egypt*
[b]*Chemical Industries Institute, National Research Centre, Dokki, 12622, Cairo, Egypt*
[c]*Pharmacology Unit, Cancer Biology Department, National Cancer Institute, Cairo University, Cairo, Egypt*
[d]*Therapeutic Chemistry Department, Pharmaceutical and Drug Industries Research Institute, National Research Centre, Dokki, 12622, Cairo, Egypt. E-mail: aisha_pharmacy@yahoo.com*

† Electronic supplementary information (ESI) available. See DOI: https://doi.org/10.1039/d4ra06146b

© 2024 The Author(s). Published by the Royal Society of Chemistry

Open Access Article. Published on 07 October 2024. Downloaded on 2/11/2026 10:58:08 AM. This article is licensed under a Creative Commons Attribution-NonCommercial 3.0 Unported Licence.

will result in many diseases such as autoimmune, cardiovascular, and neurological diseases as well as cancers. Consequently, the development of PKIs may serve as a treatment method for related diseases.[7]

The complicated nature of cancer implies the use of multi-targeted kinase inhibitors, where a single compound targets more than one kinase that were previously reported to have cross-linked pathways (this is due to a certain percentage of the ATP binding sites being conserved), in an attempt to obtain a synergistic effect, with fewer side effects and to overcome drug resistance.[4,8,9]

An example of the serine/threonine kinase family is the cyclin-dependent kinases (CDKs), which are responsible for cell cycle progression and control cellular division, proliferation, gene transcription, protein synthesis and finally cell death.[10] One of the CDK isoforms is CDK2, whose activation requires its binding with one of its regulatory subunits cyclin A or E to be able to share in the essential cellular processes.[10] Furthermore, various types of cancers, such as hepatic, pancreatic, ovarian, melanoma, cervical and breast cancers, are linked to dysregulation of CDK2 or its cyclins.[11] Based on the promising outcomes of marketed CDK2 inhibitors on tumour cells, CDK2 can be considered a valuable target in the drug discovery of cancer-targeting therapeutics.[12–14]

Another example of the constitutive serine/threonine kinase family is glycogen synthase kinase (GSK3), a multi-functioning kinase, which controls glycogen metabolism as well as involves in many cellular processes, including the cell cycle, gene transcription, proliferation, metabolism and cell death (including apoptosis and autophagy). It presents in two isoforms: GSK3α (alpha) and GSK3β (beta).[15] Particularly, the dysregulation in GSK3β activity was reported in neurological, metabolic and neoplastic diseases.[16] A literature survey revealed that GSK3β is a valuable therapeutic target in more than twenty types of malignancies.[17] Moreover, there is growing evidence that emphasizes the protective role of GSK3β inhibitors on normal cells from the adverse side effects of conventional tumour therapies and their important role in managing radio-resistance and chemoresistance.[18] Therefore, the design of novel GSK3β inhibitors is considered a valuable approach in tumour-targeting therapies.[19]

The molecular hybridization drug design approach is widely used in medicinal chemistry research in which two or more therapeutically active pharmacophores are combined to obtain a novel single compound with an expected greater therapeutic effect.[20]

Pyridine, as a core structure, has been found in a wide range of pharmacologically active synthetic or natural compounds, which has anti-proliferative,[21] antimicrobial, and anti-hepatitis B virus[22] actions and is a promising candidate in the management of cardiovascular disorders.[23] When pyridine carbonitrile was hybridized with methyl benzenesulfonamide in compound **A** (Fig. 1), it afforded a CDK2 inhibitor with $IC_{50} = 1.79$ μM and with anti-proliferative activity against MCF-7 with $IC_{50} = 18.3$ μM.[24] In compound **B**, pyridine was hybridized with thiazolidin-4-one-triazole-glycoside through an ethylidenehydrazono spacer to afford a CDK2 inhibitor with $IC_{50} = 0.18$ μM and good anti-proliferative activity against HepG2 and MCF-7 with $IC_{50} = 2.09$ and 0.15 μM, respectively.[25] Moreover, there are a lot of promising pyridines incorporating GSK3β inhibitors in different clinical phases, such as CHIR99021 (ref. 26) (pan GSK3), AZD1080,[27] and AZD2858,[28] in addition to the newly reported potent bi-pyridine single-digit GSK3β inhibitor in compound **C** with $IC_{50} = 3.4$ nM.[29]

Compounds containing thiazole, dihydrothiazol or thiazolidinone core have a wide range of therapeutic activities, such as anticancer,[30] antibacterial,[31] antifungal,[32] anticonvulsant[33] and anti-inflammatory[34] actions. SNS-032, with thiazole as a central core structure, is a potent and selective CDK2 inhibitor with $IC_{50} = 48$ nM.[35] The 4-thiazolidinone compound **D** showed CDK2 inhibitory activity with $IC_{50} = 0.63$ μM and induced apoptosis in the MCF-7 cell line.[36] A potent selective GSK3β inhibitor incorporating a thiazolidinedione core structure is tideglusib with $IC_{50} = 60$ nM.[37] New compounds **E** and **F** with a thiazolidinedione core structure and hydrazono linker were reported as GSK3β inhibitors with $IC_{50} = 180$ and 0.71 μM, respectively[29] (Fig. 1).

Based upon the aforementioned findings, we designed a series of twenty-six novel pyridine-2,3-dihydrothiazole and pyridine-thiazolidin-4-one hybrids through an ethylidenehydrazono spacer, as presented in Fig. 2. The newly synthesized derivatives were evaluated for their anti-proliferative activities against hepatocellular, breast and laryngeal carcinoma cell lines, which were previously reported to overexpress CDK2 (ref. 38–40) and GSK3β[41–43] as well as were evaluated against the normal African green monkey kidney cell line in order to detect their safety limits. The promising compounds were investigated for their *in vitro* inhibition of CDK2/cyclin A and GSK3β, as well as their effect on the cell cycle, apoptosis, caspase-3, Bax and Bcl-2 proteins. An *in silico* study of the promising compounds was performed, including ADME and molecular docking in the ATP-binding pocket of CDK2 and GSK3β, to predict the binding affinity and binding interactions with the amino acid residues in the active sites.

2 Results and discussion

2.1. Chemistry

The current work synthesized two kinds of substituted 1,3-thiazoles, **1** and **2**, connected to the pyridine moiety (Scheme 1).

A facile synthesis of the key (*E*)-2-(1-(pyridin-2-yl)ethylidene) hydrazine-1-carbothioamide **1a** was prepared *via* the reaction of **2** acetyl pyridine with thiosemicarbazide in the presence of conc. HCl following a previously described method.[44] The alkyl thiosemicarbazide derivative **1b** was synthesized with high yields through the reaction of **2** acetyl pyridine with ethyl thiosemicarbazide in the presence of a catalytic amount of HCl following a previously described method.[45] The Hantzsch

 © 2024 The Author(s). Published by the Royal Society of Chemistry

Open Access Article. Published on 07 October 2024. Downloaded on 2/11/2026 10:58:08 AM.
This article is licensed under a Creative Commons Attribution-NonCommercial 3.0 Unported Licence.

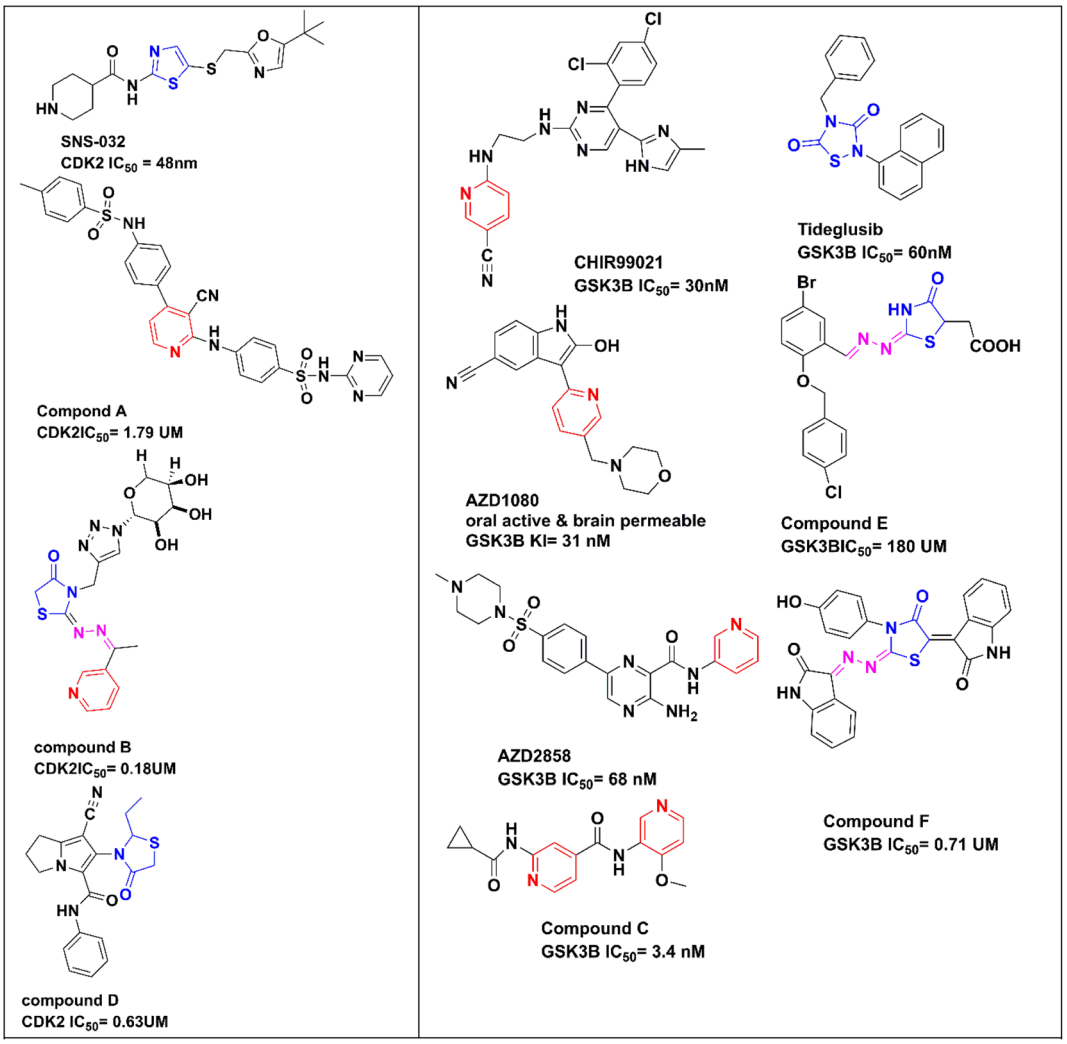

Fig. 1 Promising CDK2 inhibitors and GSK3β inhibitors.

reaction of thiosemicarbazones derivatives **1a,b** with chloroacetone, chloroacetyl acetone, phenacyl bromide, or 4-bromo phenacyl bromide in absolute ethanol and fused sodium acetate under reflux led to the new pyridine-2,3-dihydrothiazole derivatives **2a,b–5a,b**, respectively (Scheme 1). Compounds **4a** and **5a** were prepared using a previously described method.[46,47] ^{1}H NMR spectra of compounds **2b**, **3b**, **4b**, and **5b** contained no signals of the NH groups recorded in the ethylthiosemicarbazide derivatives of their precursors. Compounds **2a**, **2b**, **4b** and **5b** demonstrated the singlet attributed to the CH of the thiazole ring at 6.04–6.44 ppm. The IR spectra for the previous derivatives **3a** and **3b** showed the presence of a carbonyl group as evidence for the formation of the new derivatives at 1632 and 1625 cm^{-1}. Moreover, the ^{13}C NMR spectra for derivatives **3a** and **3b** showed characteristic signals for C=O at 190.95 ppm.

The reaction of thiosemicarbazone derivatives **1a** and **1b** with ethyl bromoacetate, ethyl-2-bromopropionate or ethyl-2-chloroacetoacetate prepared pyridin-2-yl-thiazolidin-4-one derivatives **6a,b–8a,b**, respectively (Scheme 2). Compound **6a**

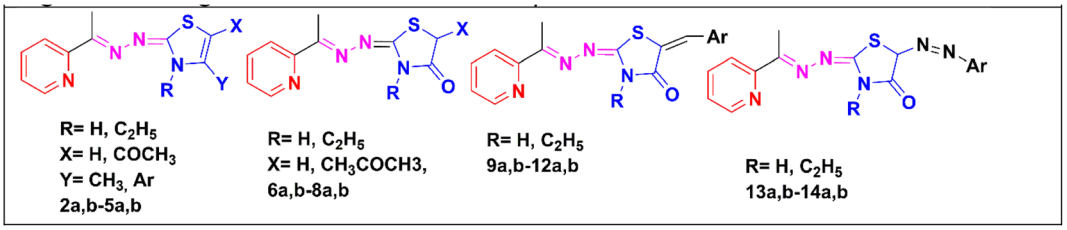

Fig. 2 The newly designed pyridine-2,3-dihydrothiazole and pyridine-thiazolidin-4-one hybrids using a molecular hybridization approach.

Open Access Article. Published on 07 October 2024. Downloaded on 2/11/2026 10:58:08 AM.
This article is licensed under a Creative Commons Attribution-NonCommercial 3.0 Unported Licence.

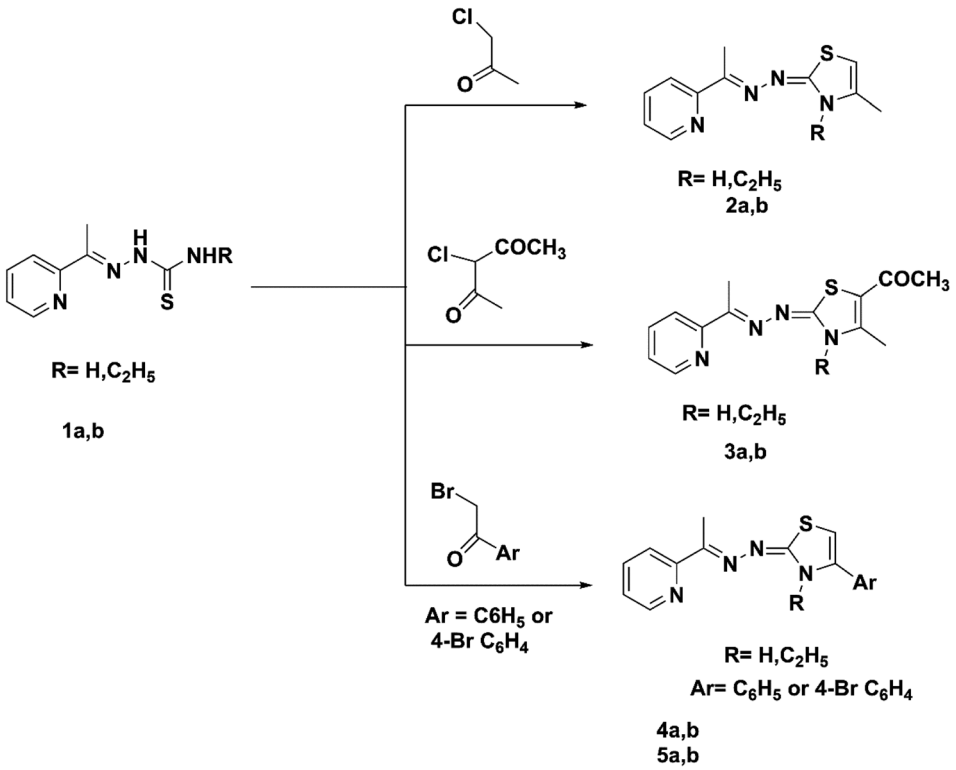

Scheme 1 Synthesis of pyridin-2-yl-2,3-dihydrothiazole hybrids (2a,b–5a,b).

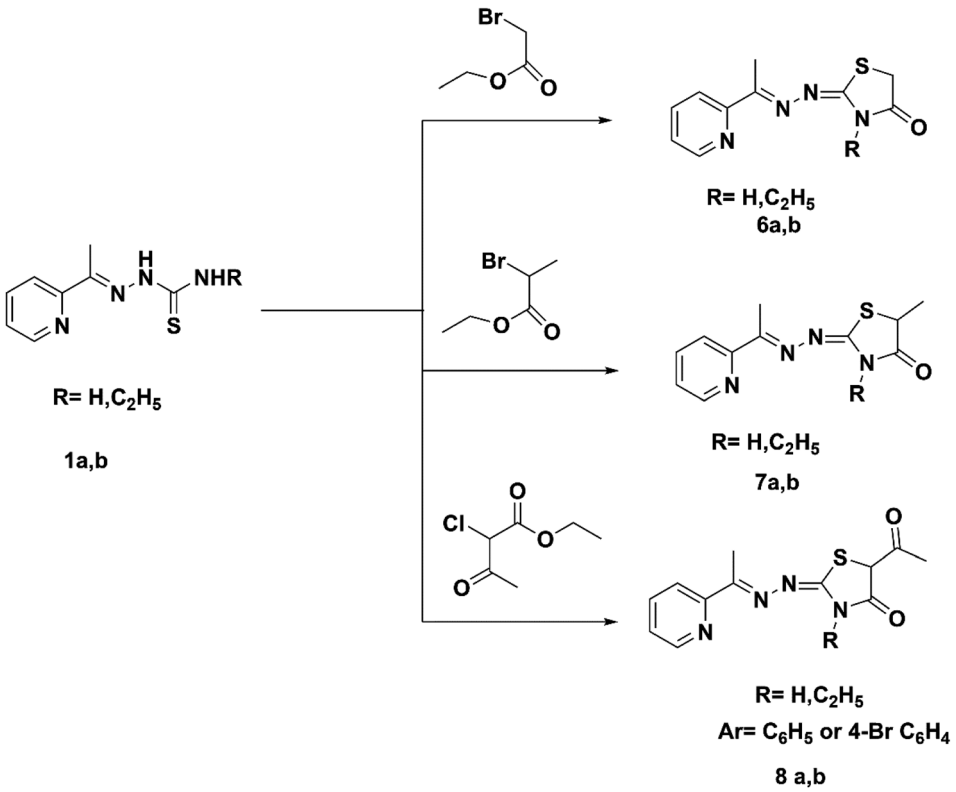

Scheme 2 Synthesis of pyridin-2-yl-thiazolidin-4-one hybrids (6a,b–8a,b).

 © 2024 The Author(s). Published by the Royal Society of Chemistry

Open Access Article. Published on 07 October 2024. Downloaded on 2/11/2026 10:58:08 AM. This article is licensed under a Creative Commons Attribution-NonCommercial 3.0 Unported Licence.

was prepared using a previously described procedure.[25] The IR spectrum of compound **6b** exhibited bands at 1715 cm^{-1} (C=O). The ^{1}H NMR spectra of compounds **7a** and **7b** exhibited the quartet of CH of the thiazole ring at 4.13 and 4.22 ppm. The ^{1}H NMR spectra of **8a** and **8b** exhibited the singlet signal of CH of the thiazole ring at 4.17 and 4.17 ppm. The ^{13}C NMR spectra of hydrazonothiazolidin-4-one derivatives **6b–8a,b** showed characteristic signals for C=O at 170.64–176.23 ppm.

Thiosemicarbazones **1a** and **1b** were allowed to react with ethyl bromoacetate and an equimolar amount of an appropriate aromatic aldehyde, 4-fluorobenzaldehyde, 4-chlorobenzaldehyde, 4-methoxybenzaldehyde, or 3,4-dimethoxybenzaldehyde, in the presence of a mixture of glacial acetic acid and anhydrous sodium acetate. The pyridin-2-yl-5-substituted benzylidene-thiazolidin-4-one derivatives **9a,b–12a,b** were obtained in 70–80% yields. Another pathway for the formation of compounds **9a,b–12a,b** was based on the reaction of compounds **6a** and **6b** with aromatic aldehydes in the presence of a mixture of glacial acetic acid and anhydrous sodium acetate (Scheme 3). The ^{13}C NMR spectra of compounds **9a,b–12a,b** revealed the presence of a characteristic CH benzylic peak, recorded from their precursor thiosemicarbazide derivatives **1a** and **1b** at 142.91–143.72 ppm.

Pyridin-2-yl-5-diazenyl-2,3-dihydrothiazole derivatives **13a,b–14a,b** were formed by the reaction of compounds **1a** and **1b** and an appropriate hydrazonoyl chloride in absolute ethanol catalyzed by TEA (Scheme 3). Compound **14a** was prepared by a procedure described earlier.[48] Mass spectra of compounds **13a**, **13b** and **14b** displayed molecular ion peaks at m/z 350, 378 and 398, respectively.

2.2. Biological evaluation

2.2.1. *In vitro* anti-proliferative assay. The twenty-six compounds, including the 2 precursors **1a** and **1b**, were evaluated for their anti-proliferative activity against three cancer cell lines: human hepatocellular carcinoma cell line (HepG2), human breast carcinoma cell line (MCF-7) and human laryngeal carcinoma cell line (HEp-2) as well as one normal cell line (the African green monkey kidney cell line (Vero)) using the sulforhodamine-B (SRB) method.[49]

Firstly, the % inhibition at a single concentration (100 μg mL^{-1}) of all the tested compounds was assessed. Only the promising compounds that exhibited % inhibition > 75% at 100 μg mL^{-1} in the cancer cell lines and % inhibition < 45% against normal Vero cells were evaluated for IC_{50} (the concentration that produces 50% inhibition of cell growth). The cells were treated at different concentrations (0, 5, 12.5, 25 and 50 μg mL^{-1}) of compounds **1a**, **8a** and **13a** together with doxorubicin as a reference, as shown in Table 1 and Fig. 3. For each compound, its IC_{50} was calculated using dose–response curve-fitting models (GraphPad Prism software, version 5).

By inspecting the tabulated results, it was found that three compounds possessed excellent anti-proliferative activity (>75% inhibition): **1a** and **8a** against HEp-2 in addition to **13a** against HepG2. Fortunately, compounds **8a** (5-acetyl-thiazolidin-4-one derivative) and **13a** (5-(*p*-tolyldiazenyl-2,3-dihydrothiazole

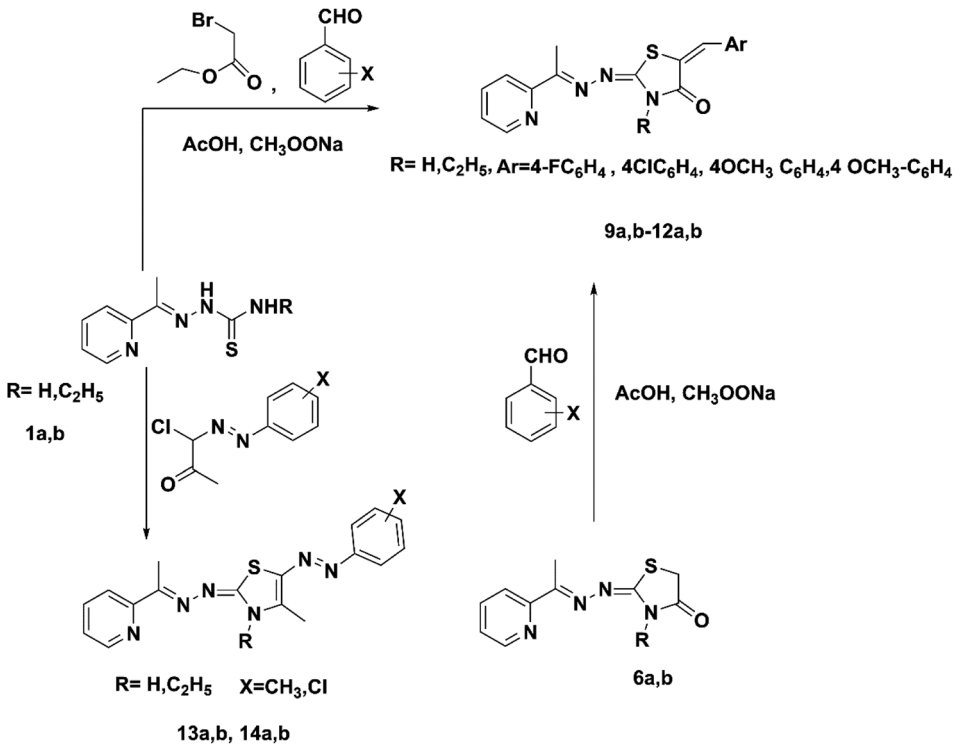

Scheme 3 Synthesis of pyridin-2-yl-5-substituted benzylidene-thiazolidin-4-one hybrids (**9a,b–12a,b**) and synthesis of pyridin-2-yl-5-diazenyl-2,3 dihydrothiazole hybrids (**13a,b–14a,b**).

Open Access Article. Published on 07 October 2024. Downloaded on 2/11/2026 10:58:08 AM.
This article is licensed under a Creative Commons Attribution-NonCommercial 3.0 Unported Licence.

Table 1 *In vitro* anti-proliferative activity of twenty-six final compounds against three human cancer cell lines MCF-7, HepG2, HEp-2 and a normal Vero cell line at a single concentration of 100 μg mL^{-1}[a]

Sample no.	MCF-7 (% inhibition)	HepG2 (% inhibition)	HEp-2 (% inhibition)	Vero (% inhibition)
1a	66.17 ± 0.9	57.62 ± 2.3	79.91 ± 0.7	61.21 ± 1.8
1b	69.85 ± 1.9	61.01 ± 1.2	69.46 ± 1.9	63.63 ± 1.5
2a	41.17 ± 2.4	72.03 ± 1.6	70.80 ± 1.7	65.45 ± 1.8
2b	70.58 ± 2.1	62.71 ± 0.8	70.44 ± 1.9	56.36 ± 1.2
3a	63.30 ± 3.3	65.25 ± 0.8	70.08 ± 1.5	63.63 ± 2.7
3b	73.52 ± 1.6	66.10 ± 1.6	71.89 ± 3.1	55.75 ± 1.9
4a	51.47 ± 1.7	67.70 ± 2.0	64.28 ± 1.7	63.63 ± 1.1
4b	53.67 ± 1.2	54.23 ± 1.6	68.12 ± 1.7	53.93 ± 1.9
5a	54.41 ± 2.0	70.31 ± 1.5	59.37 ± 3.4	57.57 ± 1.5
5b	47.79 ± 1.7	67.18 ± 1.1	58.92 ± 2.4	56.36 ± 1.7
6a	65.44 ± 1.6	60.16 ± 1.8	59.91 ± 1.8	71.51 ± 1.6
6b	63.97 ± 3.5	65.25 ± 2.5	73.21 ± 1.2	67.27 ± 1.6
7a	72.79 ± 1.3	68.64 ± 1.6	71.69 ± 1.8	69.69 ± 3.1
7b	64.70 ± 1.6	60.16 ± 0.9	74.67 ± 2.5	60.60 ± 1.6
8a	66.17 ± 1.4	68.64 ± 1.5	78.67 ± 2.5	44.24 ± 2.8
8b	63.23 ± 1.7	59.32 ± 1.9	72.44 ± 2.9	50.30 ± 1.8
9a	66.17 ± 3.1	57.627 ± 1.2	67.67 ± 2.9	57.57 ± 2.5
9b	70.58 ± 1.8	66.94 ± 1.3	74.00 ± 1.9	64.84 ± 2.1
10a	71.32 ± 3.4	61.01 ± 2.6	73.67 ± 1.2	55.75 ± 1.7
10b	59.55 ± 3.4	60.16 ± 0.9	67.18 ± 3.5	53.33 ± 3.1
11a	51.47 ± 1.4	66.94 ± 1.1	74.44 ± 3.5	61.21 ± 1.5
11b	65.44 ± 1.8	62.71 ± 3.1	74.67 ± 1.6	56.96 ± 2.9
12a	65.44 ± 3.4	60.16 ± 1.6	71.46 ± 3.4	55.75 ± 1.2
12b	61.02 ± 1.9	69.79 ± 1.7	62.50 ± 3.1	52.72 ± 0.9
13a	67.64 ± 1.0	76.56 ± 1.3	70.98 ± 1.6	41.81 ± 2.3
13b	52.94 ± 0.59	66.14 ± 2.7	61.16 ± 2.1	66.66 ± 2.2
14b	53.67 ± 0.9	68.75 ± 2.6	61.60 ± 1.7	62.42 ± 2.4

[a] Vero: normal African green monkey kidney cell line; HepG2: human liver carcinoma cell line; HEp-2: human laryngeal carcinoma cell line; MCF-7: human breast carcinoma cell line. Values are the means ± SD of three independent experiments performed in triplicate. Yellow: excellent effect (>75% inhibition), orange: good activity (>70% inhibition), not highlighted moderate effect (50–70% inhibition) and brown: weak activity.

derivative) showed a good safety profile against the normal Vero cells (<45% inhibition) with higher selectivity towards HEp-2 and HepG2 cancer cell lines, respectively, which was not the case in compound **1a**, the pyridine-thiourea precursor (Fig. 3C). Moreover, compound **13a** exhibited good anti-proliferative activity against HEp-2 (70.98% inhibition). However, the presence of an *N*-ethyl moiety in the 2,3-dihydrothiazole derivative **13b** resulted in a decrease in anti-proliferative activity against HepG2 and HEp-2, along with higher toxicity against the normal Vero cell line. The two pyridine-2,3-dihydrothiazole derivatives **2a** and **5b** showed weak anti-proliferative activities against MCF-7 with 41.17% and 47.79%, respectively, in the whole series. However, **2a** showed good anti-proliferative activity against HepG2 (72.03%) and HEp-2 (70.80%). The presence of *N*-ethyl-2,3-dihydrothiazole derivative **2b** showed good % inhibition against MCF-7 (70.58%) and retained a good % inhibition against HEp-2 (70.44%) as **2a**. In addition to compound **2b**, in the whole series, compounds **3b** (5-acetyl-2,3-dihydrothiazole derivative), **7a** (5-methyl-thiazolidin-4-one derivative), **9b** and **10a** (5-substituted-benzylidene-thiazolidin-4-one derivatives) showed good anti-proliferative activity against MCF-7 (>70% inhibition). The rest of the compounds (excluding **2a** and **5b**) showed moderate anti-proliferative activity (50–70% inhibition). Regarding the HepG2 cell lines, all of the tested compounds showed moderate cytotoxic activity, except that **13a** was excellent and **2a** and **5a** showed good activity. In the case of HEp-2, for the anti-proliferative activity of the tested compounds, two compounds **1a** and **8a** showed excellent inhibitory activity, and **14** compounds showed good inhibitory activity, namely **2a**, **2b**, **3a**, **3b** (2,3-dihydrothiazole derivatives) **6b**, **7a**, **7b**, **8b** (thiazolidin-4-one derivatives), **9b**, **10a**, **11a**, **11b**, **12a** (5-substituted-benzylidene-thiazolidi-4-one), and **13a** (5-(*p*-tolyldiazenyl-2,3-dihydrothiazole derivative). The rest of the compounds showed moderate cytotoxic activity.

As presented in the dose–response curves (Fig. 3A–C), compounds **8a** and **1a** showed anticancer activity against the HEp-2 cell line with IC_{50} of 5.9 and 7.5 μg mL^{-1}, respectively. Conversely, compound **13a** showed anticancer activity against HepG2 with IC_{50} = 9.5 μg mL^{-1}.

2.2.2. Determination of the oxidative stress of promising compounds 8a and 13a. The cells of HEp-2 and HepG2 were cultured in T75 flasks for 24 h and were then treated with IC_{50} of compounds **8a** and **13a**, respectively, for 48 h. The medium was collected in order to measure the total nitrate/nitrite (NO_x) using the Miranda method.[50] Moreover, the cell pellets of both treated cells and the control were collected from the flask by trypsinization and used to assess the reduced glutathione (GSH) following the Ellman method.[51] The protein concentration in the medium and cell lysate was assessed using Bradford method.[52]

As depicted in Fig. 4A, compounds **8a** and **13a** significantly increased the NO_x level compared to untreated cells by 19% and 25%, respectively. Moreover, there was a slight reduction in the GSH content by 14% in HEp-2 and a significant reduction in the GSH level in HepG2 cells by 33% compared to untreated cells

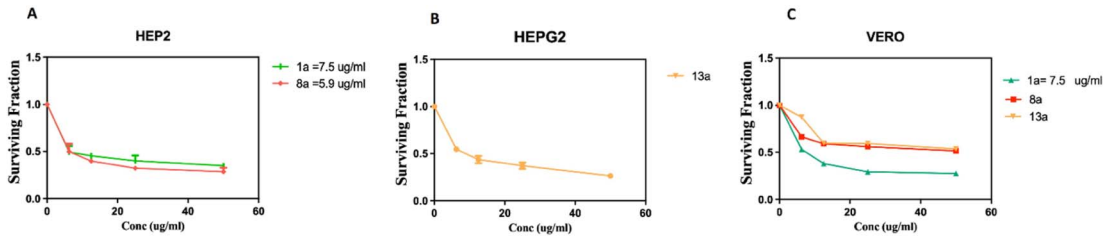

Fig. 3 Cytotoxicity of the promising compounds: (A) **1a**, **8a** against the HEp-2 cell line; (B) **13a** against the HepG2 cell line; (C) **1a**, **8a**, **13a** against the Vero cell line after 48 h. The values represents the means ± SD of three independent experiments performed in triplicate.

 © 2024 The Author(s). Published by the Royal Society of Chemistry

Open Access Article. Published on 07 October 2024. Downloaded on 2/11/2026 10:58:08 AM.
This article is licensed under a Creative Commons Attribution-NonCommercial 3.0 Unported Licence.

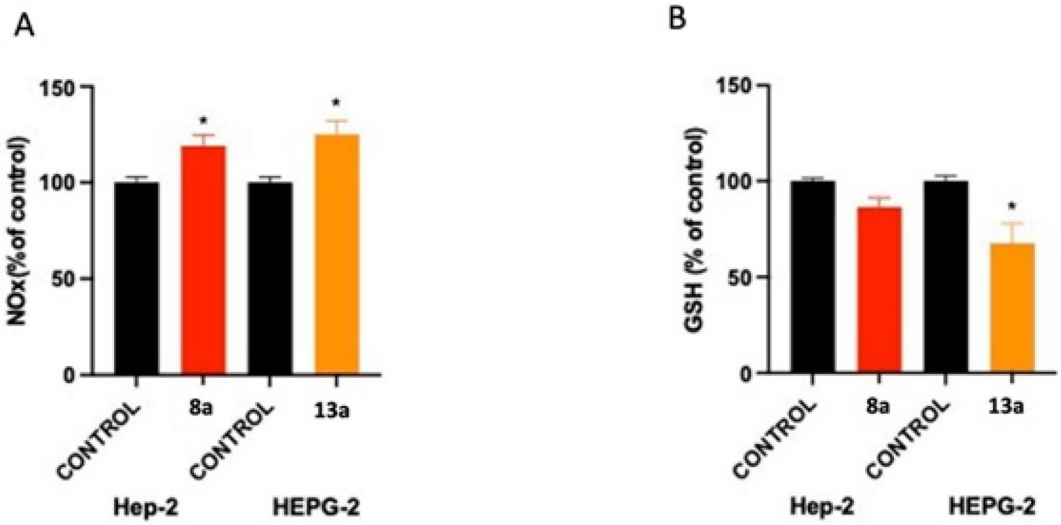

Fig. 4 Effect of treatment with **8a** and **13a** on oxidative stress and antioxidants in HEp-2 and HepG2 cell lines, respectively: NO_x (A), GSH level (B). Data are expressed as means ± SD of two independent experiments. *Compounds are significantly different from the control group at a *P* value < 0.05.

(Fig. 4B). It was noticed that the production of reactive oxygen species (ROS) was elevated after treatment with **8a** and **13a**, resulting in the induction of nuclear damage, which might also lead to an increase in apoptotic protein expression. Therefore, it can be concluded that **8a** and **13a** possess strong chemopreventive potential.

2.2.3. *In vitro* enzymatic inhibitory evaluation against CDK2 and GSK3β. The three promising compounds in terms of anti-proliferative activity, namely **1a** (pyridine-thiourea) precursor, **8a** (5-acetyl-thiazolidin-4-one) derivative and **13a** (5-(*p*-tolyldiazenyl-2,3-dihydrothiazole)) derivative were chosen for a study of *in vitro* enzymatic inhibitory activity against CDK2/cyclin A[53] and GSK3β.[54] The assay kits for each enzyme were purchased from the Bioscience Company. The Kinase-Glo reagent was purchased from Promega. This luminescent kinase assay technique detects the ATP released from the kinase reaction, which is converted to light and can be detected spectrophotometrically. The IC_{50} values (μg mL^{-1}) are described in Table 2 using roscovitine and CHIR-99021 as references, respectively.

Table 2 *In vitro* enzymatic inhibitory activity of the three promising cytotoxic compounds **1a** (pyridine-thiourea) precursor, **8a** (5-acetyl-thiazolidin-4-one) derivative and **13a** (5-(*p*-tolyldiazenyl-2,3-dihydrothiazole)) derivative against CDK2/cyclin A and GSK3β[a]

	IC_{50} (mean ± SEM) (μg mL^{-1})	
Cpd	CDK2/cyclin A	GSK3β
1a	3.25	0.438
8a	0.675	0.134
13a	0.396	0.118
Roscovitine	0.88	—
CHIR-99021	—	0.07

[a] IC_{50}: compound concentration necessary to inhibit the enzyme activity by 50%; SEM: standard error of the mean; each value is the mean of three values; (—) not detected.

According to the results in Table 2, compounds **13a** and **8a** showed stronger inhibitory activity against CDK2/cyclin A by 2.2 fold and 1.3 fold compared with roscovitine. Unfortunately, **1a** (the pyridine-thiourea) precursor exhibited the weakest activity with roscovitine demonstrating more than 3.5 times its inhibitory activity. In the case of GSK3β inhibitory activity, the three tested compounds showed moderate inhibitory activity, with **13a** and **8a** showing approximately twice the CHIR-99021 inhibitory activity. However, **1a** showed very weak inhibitory activity with the reference drug showing nearly six times its inhibitory activity. Thus, it can be concluded that **13a** exhibited anti-proliferative activity against HepG2 by acting as a dual CDK2 (strong)/GSK3β (moderate) inhibitor. Moreover, **8a** showed anti-proliferative activity against HEp-2 by acting as a dual CDK2/GSK3β inhibitor but was slightly weaker than **13a**. The pyridine-thiourea precursor **1a** showed excellent anti-proliferative activity against HEp-2 but was the weakest dual CDK2/GSK3β inhibitor.

2.2.4. Cell cycle analysis and apoptosis of compound 13a. To investigate whether compound **13a** (pyridine-5-(*p*-tolyldiazenyl-2,3-dihydrothiazole)) derivative induced its cytotoxic effect *via* apoptosis, HepG2 cells were treated with 9.5 μg mL^{-1} (IC_{50}) for 24 h. The cells were then stained with an annexin V/PI commercial kit (Becton Dickenson, Franklin Lakes, NJ, USA) according to the manufacturer's instructions and screened through flow cytometry (Fig. 5–7). Cell cycle phases were determined using a fluorescent dye to stain the DNA followed by measuring its intensity. Staining of DNA displays a clear differentiation of the cells in different stages, such as the G0/G1 phase, S, G2 and M phases, in addition to the evaluation of aneuploid sets of cells. Cell cycle analysis was performed with a Beckman Coulter (Brea, CA, USA) analyzer.[55]

Open Access Article. Published on 07 October 2024. Downloaded on 2/11/2026 10:58:08 AM.
This article is licensed under a Creative Commons Attribution-NonCommercial 3.0 Unported Licence.

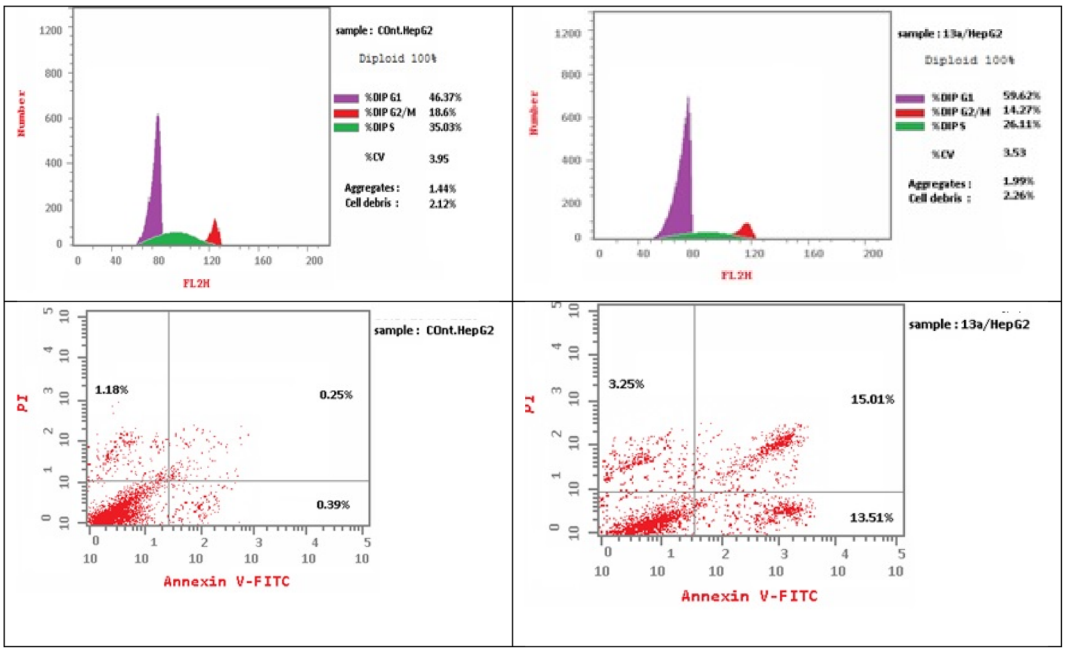

Fig. 5 Cell cycle analysis and the effect of the pyridine-5-(*p*-tolyldiazenyl-2,3-dihydrothiazole) hybrid **13a** on the percentage of V-FITC-positive annexin staining in HepG2 cells compared with the control.

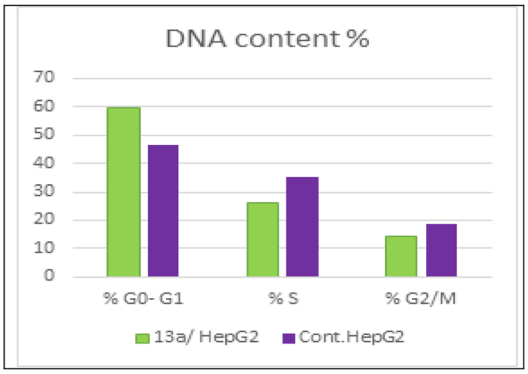

Fig. 6 Cell cycle analysis of pyridine-5-(*p*-tolyldiazenyl-2,3-dihydrothiazole) hybrid compound **13a**.

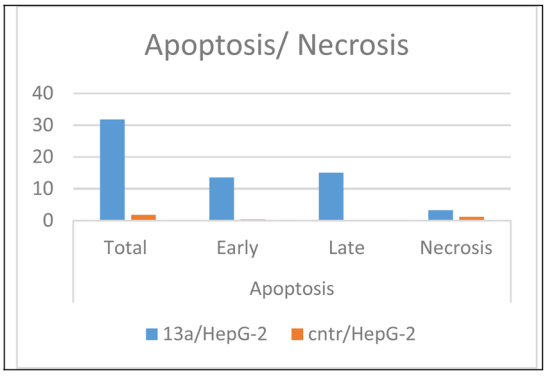

Fig. 7 Apoptotic activity of pyridine-5-(*p*-tolyldiazenyl-2,3-dihydrothiazole) hybrid compound **13a**.

As presented in Fig. 6, compound **13a** caused cell accumulation of 59.62% in the G0–G1 phase compared with untreated HepG2 cells. Therefore, compound **13a** caused G1 cell cycle arrest. Moreover, there was an elevation in the total number of apoptotic cells by 31.77% compared with 1.82% for the DMSO control, as shown in detail in Fig. 6 (% of early and late apoptosis). Additionally, it is noticeable that the % of necrotic cells was 3.25% in **13a**-treated HepG2 cells compared with 1.18% in the DMSO control. All of these results pointed to the ability of compound **13a** to induce apoptosis.

2.2.5. The effect of compounds 13a on the levels of Bax, Bcl-2 and caspase-3 in HepG2 cells. Apoptosis is performed by two main routes. The first is the mitochondrial (intrinsic) route, which is regulated by pro-apoptotic Bax and anti-apoptotic Bcl-2 proteins. The second is the cytoplasmic (extrinsic) route, which is controlled by cell surface death receptors, such as FAS, TNF-α and TRAIL (TNF-related apoptosis inducing ligand). Both routes lead to the activation of caspases (such as caspase-3 or the executer protein) by enhancing permeability in the mitochondrial outer membrane and the release of mitochondrial proteins, such as cytochrome c and DIABLO/Smac proteins, in the cell cytoplasm. Besides these previous steps, condensation of chromatin and DNA fragmentation are performed during apoptosis causing cell destruction.[56,57]

In the present study, major apoptotic parameters were evaluated to trace the anti-proliferative (or apoptosis induction) effect of compound **13a** on HepG2 cancer cells. The gene expression of the pro-apoptotic protein Bax[58] and the anti-apoptotic protein Bcl-2 (ref. 59) in addition to the death protein caspase-3 (ref. 60) were evaluated using the RT-PCR technique.

 © 2024 The Author(s). Published by the Royal Society of Chemistry

Open Access Article. Published on 07 October 2024. Downloaded on 2/11/2026 10:58:08 AM.
This article is licensed under a Creative Commons Attribution-NonCommercial 3.0 Unported Licence.

Table 3 The effect of compound **13a** on Bax, Bcl-2 and caspase 3

		RT-PCR fold change		
Compound	Cells	Bax	Bcl-2	Caspase 3
13a/HepG2	HepG2	4.337	0.303	4.916
Control HepG2	HepG2	1	1	1

As shown in Table 3, after the treatment of HepG2 cells with 9.5 μg mL^{-1} (IC_{50}) for 24 h, there was a 4.33-fold increase in Bax protein and a decrease in Bcl-2 protein by a value equal to 0.3 fold in **13a**/HepG2 treated cells compared to the control untreated HepG2 cancer cells. Additionally, an increase in the caspase-3 gene expression by a value equal to 4.9 fold was observed in **13a**/HepG2 compared to its corresponding control. These results pointed to the impact of compound **13a** in inducing apoptosis in the HepG2 cancer cell.

2.3. *In silico* study of promising compounds 1a, 8a and 13a

Based on the promising *in vitro* biochemical screening results, three compounds were selected for further *in silico* study comprising ADME prediction and a docking study in the ATP binding pocket of CDK2 and GS3Kβ.

2.3.1. *In silico* prediction of drug likeness, ADME studies. Predictions of some physicochemical properties and pharmacokinetic parameters (including absorption, distribution, metabolism and excretion) of promising compounds **1a**, **8a**, and **13a** were estimated using the SwissADME website (**https://www.swissadme.ch**),[61] as demonstrated in Table 4 and Fig. 7.

Favourably, the three tested compounds were predicted to fulfil the Pfizer Lipinski rule of five without any violation.[62] Additionally, the water solubility was predicted as having Ali log *S* scale values ranging from ≤10 insoluble to ≤2 soluble, where **1a** and **8a** were very soluble and **13a** showed moderate solubility.[63] According to Fig. 8, the boiled-egg plot[64] showed that the three compounds were expected to be highly absorbed from the gastrointestinal tract and would not cross the blood–brain barrier, and they were not expected to be a substrate for the efflux transporter P-glycoprotein.

2.3.2. Molecular docking simulation study. For deeper visualization of the binding energy scores and interactions of the three promising compounds **1a**, **8a** and **13a** in the ATP-binding pocket of both enzymes CDK2 and GSK3β, a molecular docking simulation study was carried out using Autodock

Table 4 SwissADME predictions of drug likeness (Lipinski rule) with other physicochemical properties including water solubility (Ali log *S*) for compounds **1a**, **8a** and **13a**[a]

	Lipinski rules						Violation	Water solubility	
Compound	MW ≤ 500	HB acceptor ≤ 10	HB donor ≤ 5	TPSA	MLOGP ≤ 4.15	Rotatable bonds ≤ 9	Yes or 0	Ali log *S*	Ali class
1a	194.26	2	2	95.39	−0.14	3	0	−2.31	Very soluble
8a	276.31	5	1	109.08	−0.14	3	0	−2.31	Very soluble
13a	350.44	5	1	106.36	2.19	4	0	−6.33	Moderate

[a] MW: molecular weight ≤ 500; log *P*: lipophilicity < 4.15; HBA: hydrogen bond acceptor ≤ 10; HBD: hydrogen bond donor ≤ 5; TPSA (topological polar surface area) 20–130 $Å^2$.

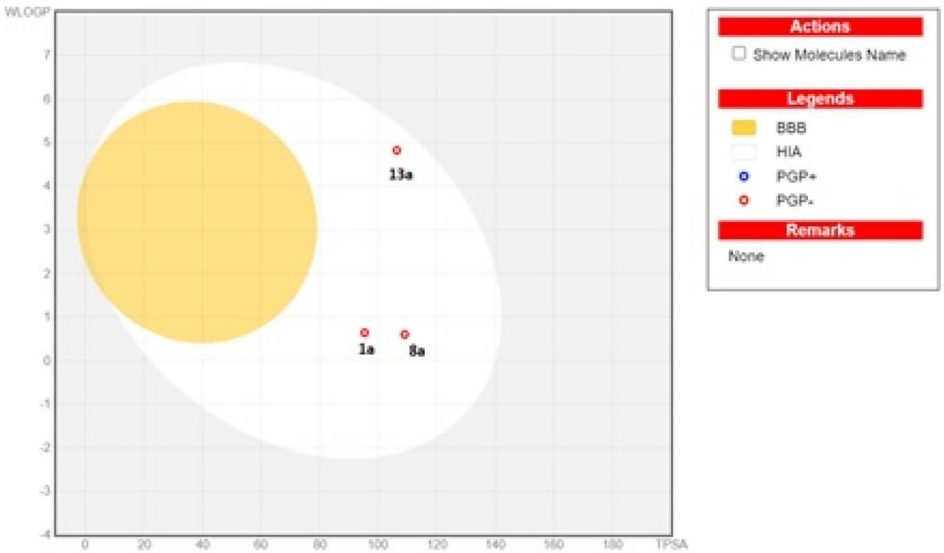

Fig. 8 Boiled-egg plot from the SwissADME website for compounds **1a**, **8a** and **13a**.

Open Access Article. Published on 07 October 2024. Downloaded on 2/11/2026 10:58:08 AM.
This article is licensed under a Creative Commons Attribution-NonCommercial 3.0 Unported Licence.

Table 5 The binding affinity (kcal mol^{-1}) for the three promising compounds **1a**, **8a** and **13a** and the native ligands in the CDK2 and GSK3β kinase domain

Compound	Binding affinity (kcal mol^{-1}) CDK2	Binding affinity (kcal mol^{-1}) GSK3β
1a	−6.4	−5.5
8a	−8.2	−7.8
13a	−8.6	−8.0
AZD5438	−8.6	—
2WF	—	−8.6

Vina Wizard PyRx (https://pyrx.sourceforge.io/)[65] following a previously reported method.[66] The Protein Data Bank (https://www.rcsb.org/) was the source of the downloaded 3D structure of the targeted kinase co-crystallized with a native ligand inhibitor as follows: CDK2 (PDB ID 6GUH)[67] and GSK3β (PDB ID 4PTE).[68] The YASARA energy minimization server[69] was used after protein preparation for kinase energy minimization. For validation of the docking process, the native ligand was re-docked in each kinase with the tested compounds, where the RMDS was 0.1 and 0.2 Å, respectively. Biovia Discovery Studio 2021 (https://discover.3ds.com/) was

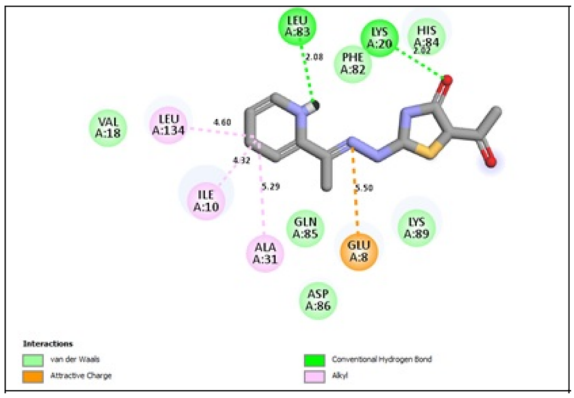

Fig. 10 2D binding interactions of compound **8a** in CDK2.

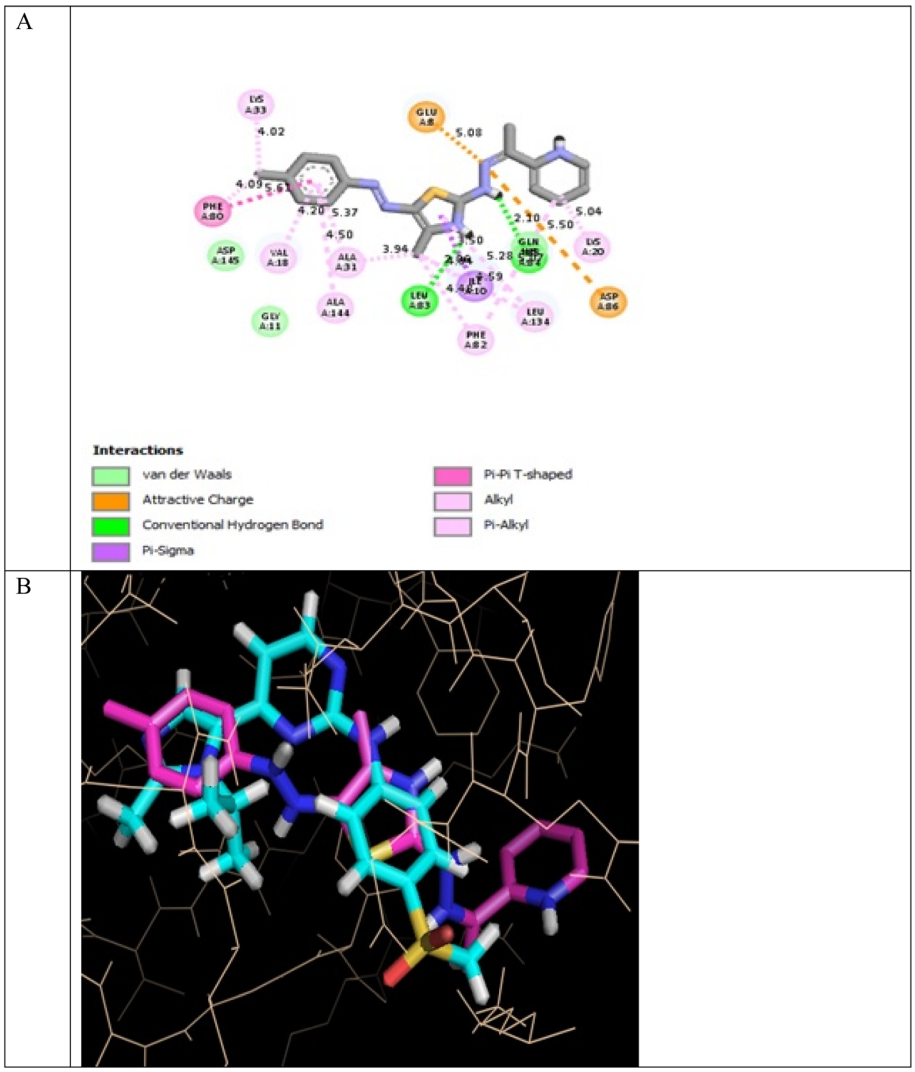

Fig. 9 (A) 2D binding interactions of compound **13a** in CDK2 (PDB ID 6GUH), (B) 3D structure of **13a** (pink) superimposed with AZD5438 (pink) in CDK2 (PDB ID 6GUH) in tint sticks.

 © 2024 The Author(s). Published by the Royal Society of Chemistry

Open Access Article. Published on 07 October 2024. Downloaded on 2/11/2026 10:58:08 AM.
This article is licensed under a Creative Commons Attribution-NonCommercial 3.0 Unported Licence.

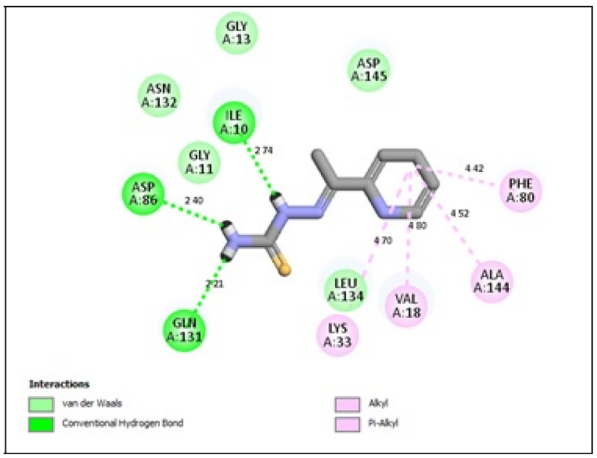

Fig. 11 2D binding interactions of compound **1a** in CDK2.

used in reporting the 2D and 3D binding interactions. The binding affinities of the tested compounds and the native ligand are tabulated in Table 5.

In the CDK2 ATP binding site, it was predicted that **13a** had the highest binding affinity (−8.6 kcal mol^{-1}), which was similar to that of the native ligand AZD5438 (−8.6 kcal mol^{-1}), followed by **8a** (−8.2 kcal mol^{-1}). Both were superior to **1a** (−8.2 kcal mol^{-1}), the pyridine thiourea precursor (Table 5). Regarding the binding interactions (Fig. 9A and B), compound **13a** formed two hydrogen bonds with Leu83 (2.06 Å) and His84 (2.10 Å) considering that the interaction with Leu83 in the hinge region is essential, as previously reported. Additionally, there were several hydrophobic interactions, including pi–pi interaction with Phe80 (5.61 Å), pi–sigma interaction with Ile10 (3.5 Å), several pi–alkyl interactions and van der Waals interactions (Fig. 9A). In Fig. 9B, compound **13a** was typically superimposed over AZD5438 with the pyridine ring extension in the binding

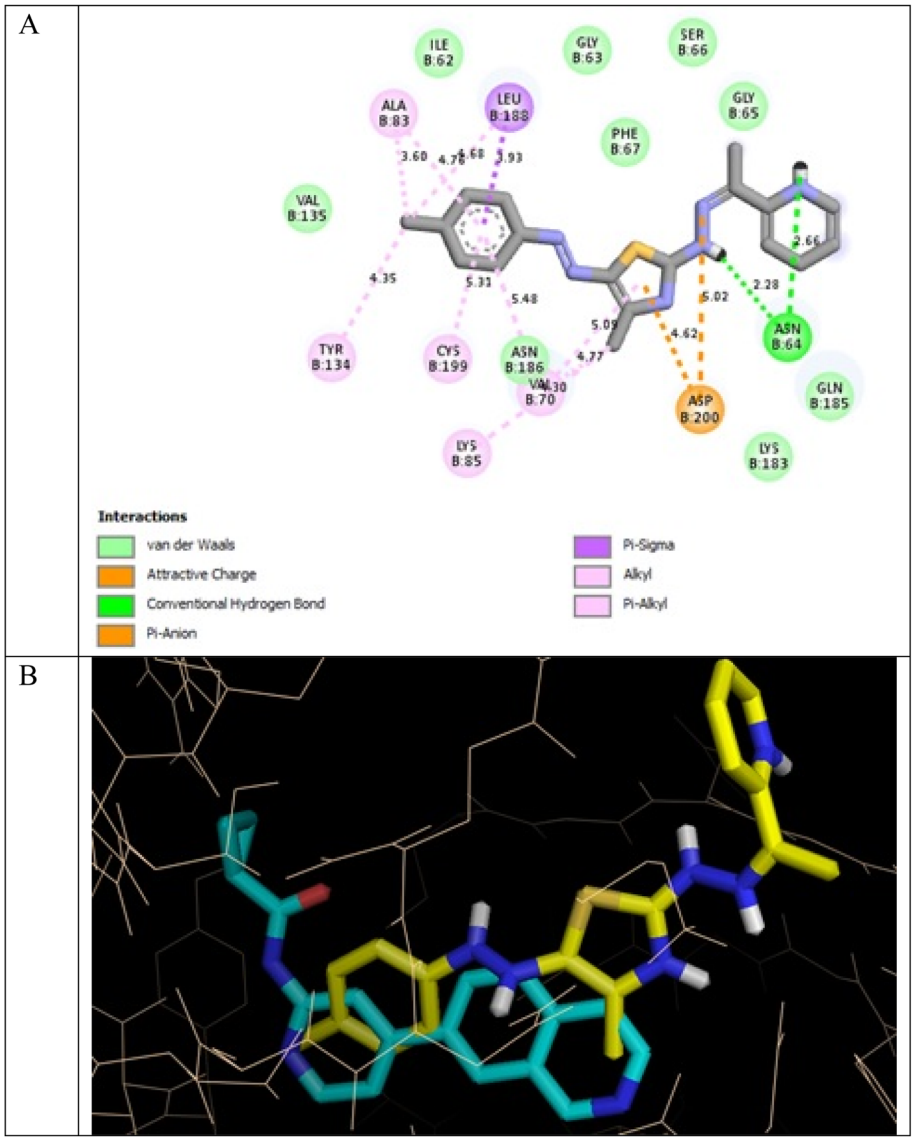

Fig. 12 (A) 2D binding interactions of compound **13a** in GSK3β (PDB ID 4PTE); (B) 3D structure of **13a** (yellow) superimposed with 2WF (cyan) in GSK3β (PDB ID 4PTE) in tint sticks.

Open Access Article. Published on 07 October 2024. Downloaded on 2/11/2026 10:58:08 AM.
This article is licensed under a Creative Commons Attribution-NonCommercial 3.0 Unported Licence.

site forming more hydrophobic interactions, which may increase the stability of the compound in the pocket. In Fig. 10, compound **8a** formed two hydrogen bonds one with the essential Leu83 (2.08 Å) and the other with Lys20 (2.02 Å), in addition to hydrophobic alkyl and van der Waals interactions. Compound **1a** formed three hydrogen bonds with Ile10 (2.74 Å), Asp86 (2.40 Å) and Gln131 (2.21 Å) with the NH of the thiourea moiety, highlighting the previously reported essential Asp86 interaction in the hinge region, but this interaction was not sufficient to potently inhibit CDK2 (Fig. 11).

In conclusion, the docking simulation study coincides with the *in vitro* enzymatic assay, which pointed out that **13a** was the most potent CDK2 inhibitor among the tested compounds followed by **8a** and the pyridine thiourea precursor **1a** was the weakest. Therefore, hybridization of the pyridine core structure with 2,3-dihydrothiazole (**13a**) or thiazolidin-4-one (**8a**) through an ethylidenehydrazono spacer was significant for CDK2 inhibitory activity.

In the GSK3β ATP binding site, it was predicted that **13a** had the highest binding affinity (−8.0 kcal mol^{-1}) but less than that of the native ligand 2WF (−8.6 kcal mol^{-1}), followed by **8a** (−7.8 kcal mol^{-1}). Both were superior to **1a** (−5.5 kcal mol^{-1}), the pyridine thiourea precursor (Table 5).

It was reported that 2WF formed hydrogen bonds with Lys85 and Val135. Unlikely compound **13a** formed hydrophobic interactions with Lys85 and Val135 and instead formed two hydrogen bonds with Asn64 (2.28 Å and 2.66 Å). There were several hydrophobic interactions exemplified in pi–sigma interaction with Leu188 (3.93 Å), pi–anion interaction with Asp200 (4.62 Å), many pi–alkyl and van der Waals interactions, as presented in Fig. 12A. Compound **13a** was slightly superimposed, mainly the 5(*p*-tolyldiazenyl)-2,3-dihydrothiazole moiety, over the native ligand 2WF, which might explain the slight decrease in its binding affinity (Fig. 12B). It was predicted that compound **8a** would keep the essential hydrogen bond between thiazolidin-4-one carbonyl and Lys85 (3.06 Å) with alkyl and van der Waals hydrophobic interactions (Fig. 13). Conversely, although **1a** possessed three hydrogen bonds two of which were with the essential Val135, it was the weakest GSK3β

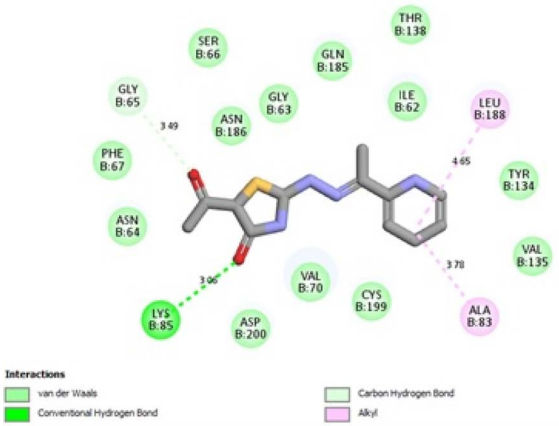

Fig. 13 2D binding interactions of compound **8a** in GSK3β (PDB ID 4PTE).

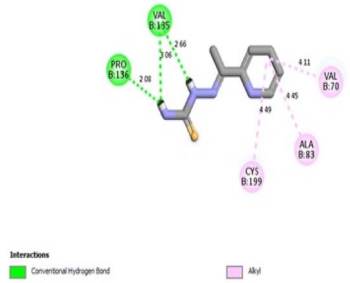

Fig. 14 2D binding interactions of compound **1a** in GSK3β (PDB ID 4PTE).

inhibitor in the tested set (Fig. 14). Depending on the agreement of the docking study results with the *in vitro* GSK3β inhibitory screening results, the importance of pyridine hybridization with 2,3-dihydrothiazole (**13a**) and with thiazolidin-4-one (**8a**) through an ethylidenehydrazono spacer was highlighted for affording a GSK3β inhibitor.

3 Conclusions

In this research, twenty-six novel hybrids were designed and synthesized as follows: pyridin-2-yl-2,3-dihydrothiazoles (**2a,b–5a,b**), pyridin-2-yl-thiazolidin-4-ones (**6a,b–8a,b**), pyridin-2-yl-5-substituted benzylidene-thiazolidin-4-ones (**9a,b–12a,b**) and pyridin-2-yl-5-diazenyl-2,3-dihydrothiazoles (**13a,b–14a,b**) as dual CDK2/GSK3β inhibitors. Almost all of the synthesized compounds including their precursors **1a** and **1b** were *in vitro* screened for anti-proliferative activity against MCF-7, HepG2, and HEp-2 cancer cell lines and the Vero normal cell lines. Compound **8a** (pyridine-5-acetyl-thiazolidin-4-one) hybrid exhibited excellent anti-proliferative activity against HEp-2, and **13a** (pyridine-5-(*p*-tolyldiazenyl-2,3-dihydrothiazole)) hybrid possessed excellent anti-proliferative activity against HepG2 with an acceptable safety profile against normal cells. Additionally, **1a** (pyridine thiourea) precursor showed excellent anti-proliferative activity against HEp-2, but it negatively affected normal cells. The three promising anti-proliferative compounds **1a**, **8a** and **13a** were evaluated for inhibitory activity against CDK2 and GSK3β using roscovitine and CHIR-99021 as references, respectively. Compound **13a** was the most potent dual CDK2/GSK3β inhibitor followed by **8a**, and the weakest was **1a**. Further study of compound **13a** revealed that it caused G1 cell cycle arrest and induced apoptosis. Moreover, it caused an increase in Bax and caspase-3 levels with a decrease in Bcl-2 levels in HepG2. Finally, an *in silico* study of the three promising compounds predicted an acceptable drug likeness and ADME profiles. The molecular modelling simulation results were in agreement with the *in vitro* kinase inhibitory results and highlighted the importance of pyridine hybridization with 2,3-dihydrothiazole (**13a**) and with thiazolidin-4-one (**8a**) through an ethylidenehydrazono spacer for dual CDK2/GSK3β inhibitory activity. These might act as promising leads which may be subjected to further modification for better anti-proliferative activity in future work.

 © 2024 The Author(s). Published by the Royal Society of Chemistry

Open Access Article. Published on 07 October 2024. Downloaded on 2/11/2026 10:58:08 AM. This article is licensed under a Creative Commons Attribution-NonCommercial 3.0 Unported Licence.

4 Experimental

4.1. Chemistry

4.1.1. Synthesis of 2-(((*E*)-1-(pyridin-2-yl)ethylidene) hydrazono)-2,3-dihydrothiazole derivatives (2a,b–5a,b). A mixture of compounds **1a** and **1b** (10 mmol) in absolute ethanol (20 mL) with anhydrous sodium acetate (20 mmol), chloroacetone, chloroacetylacetone, phenacyl bromide, or *p*-bromo phenacyl bromide (10 mmol) was refluxed for 10 hours. Following cooling, the precipitate was filtered out, repeatedly cleaned with water, dried, and recrystallized from absolute ethanol to provide the appropriate thiazole derivative.

*(E)-4-Methyl-2-(((E)-1-(pyridin-2-yl)ethylidene)hydrazono)-2,3-dihydrothiazole (**2a**).* Yield 88%; mp (110–112) °C. Analysis for $C_{11}H_{12}N_4S$ (232.31) calcd: % C, 59.87; H, 5.21; N, 24.12; S, 13.80. Found: % C, 59.85; H, 5.26; N, 24.21; S, 13.84. IR (cm^{-1}, KBr): 3344 (NH), 1551 (C=N). ^1H NMR (DMSO-d6, δ, ppm): 2.15 (s, 3H, CH_3), 2.34 (s, 3H, CH_3), 6.36 (s, 1H, CH thiazole), 7.31 (1H, t, Ar–H), 7.77 (1H, t, Ar–H), 7.96 (1H, d, Ar–H), 8.52 (1H, m, Ar–H), 11.24 (1H, s, NH). ^{13}C NMR (DMSO-d6, δ, ppm): 15.16 (CH_3), 19.64 (CH_3), 99.63 (CH_2 thiazole), 122.54, 126.30, 135.99, 147.99, 153.48, 153.92, 158.85 (Ar–C + C1, C4 thiazole), 164.57 (C=N). MS *m*/*z* (RA%): 232 (M^+) (34%).

*(E)-3-Ethyl-4-methyl-2-(((E)-1-(pyridin-2-yl)ethylidene) hydrazono)-2,3-dihydrothiazole (**2b**).* Yield 80%; mp (87–89) °C. Analysis for $C_{13}H_{16}N_4S$ (260.36) calcd: % C, 59.97; H, 6.19; N, 21.52; S, 12.31. Found: % C, 59.89; H, 6.21; N, 21.43; S, 12.45. IR (cm^{-1}, KBr): 1554 (C=N). ^1H NMR (DMSO-d6, δ, ppm): 1.21 (t, 3H, CH_3), 2.15 (s, 3H, CH_3), 2.37 (s, 3H, CH_3), 3.88 (q, 2H, CH_2), 6.04 (s, 1H, CH thiazole), 7.28 (H, t, Ar–H), 7.74 (H, t, Ar–H), 8.02 (H, d, Ar–H), 8.52 (H, d, Ar–H). ^{13}C NMR (DMSO-d6, δ, ppm): 13.46 (CH_2CH_3), 13.63 (CH_3), 13.99 (CH_3), 40.59 (CH_2CH_3), 97.44 (CH_2 thiazole), 120.15, 123.54, 136.55, 149.06, 154.96, 156.85 (Ar–C + C1, C4 thiazole), 169.87 (C=N). MS *m*/*z* (RA%): 260 (M^+) (3.55%).

*1-((E)-4-Methyl-2-(((E)-1-(pyridin-2-yl)ethylidene)hydrazono)-2,3-dihydrothiazol-5-yl)ethan-1-one (**3a**).* Yield 75%; mp (115–117) °C. Analysis for $C_{13}H_{14}N_4OS$ (274.34) calcd: % C, 56.92; H, 5.14; N, 20.42; S, 11.69. Found: % C, 56.89; H, 5.11; N, 20.39; S, 11.59. IR (cm^{-1}, KBr): 3378 (NH), 1623 (C=O), 1551 (C=N). ^1H NMR (DMSO-d6, δ, ppm): 2.36 (s, 6H, CH_3, $COCH_3$), 2.39 (s, 3H, CH_3), 7.34 (1H, t, Ar–H), 7.80 (1H, t, Ar–H), 7.82 (1H, d, Ar–H), 8.02 (1H, d, Ar–H), 11.82 (1H, s, NH). ^{13}C NMR (DMSO-d6, δ, ppm): 14.11 (CH_3), 19.09 (CH_3), 25.46 (CH_3CO), 105.77, 122.05, 127.09, 136.69, 149.03, 155.16, 158.34, 158.38 (Ar–C), 164.74 (C=N), 190.95 (C=O). MS *m*/*z* (RA%): 274 (M^+) (32%).

*1-((E)-3-Ethyl-4-methyl-2-(((E)-1-(pyridin-2-yl)ethylidene) hydrazono)-2,3-dihydrothiazol-5-yl)ethan-1-one (**3b**).* Yield 75%; mp (166–168) °C. Analysis for $C_{15}H_{18}N_4OS$ (302.40) calcd: % C, 59.58; H, 600; N, 18.53; S, 10.60. Found: % C, 59.54; H, 603; N, 18.56; S, 10.57. IR (cm^{-1}, KBr): 1625 (C=O), 1556 (C=N). ^1H NMR (DMSO-d6, δ, ppm): 1.18 (t, 3H, CH_3), 2.20, 2.22 (s, 6H, CH_3, $COCH_3$, CH_3), 2.41 (s, 3H, CH_3), 3.94 (q, 2H, CH_2), 7.38 (1H, t, Ar–H), 7.84 (1H, t, Ar–H), 7.38 (1H, d, Ar–H), 8.06 (1H, d, Ar–H), 8.37 (1H, s, NH). ^{13}C NMR (DMSO-d6, δ, ppm): 7.38 (CH_3), 13.21 (CH_2–CH_3), 20.45 (CH_3), 25.56 (CH_3CO), 42.26 (CH_2–CH_3), 106.10, 122.03, 127.09, 136.69, 149.12, 155.16, 158.34, 158.38 (Ar–C), 164.91 (C=N), 190.95 (C=O). MS *m*/*z* (RA%): 302 (M^+) (100%).

*(E)-3-Ethyl-4-phenyl-2-(((E)-1-(pyridin-2-yl)ethylidene) hydrazono)-2,3-dihydrothiazole (**4b**).* Yield 65%; mp (97–99) °C. Analysis for $C_{18}H_{18}N_4S$ (322.43) calcd: % C, 67.05; H, 5.63; N, 17.38; S, 9.94. Found: % C, 67.15; H, 5.66; N, 17.40; S, 9.96. IR (cm^{-1}, KBr): 1555 (C=N). ^1H NMR (DMSO-d6, δ, ppm): 1.14 (t, 3H, CH_3), 2.43 (s, 3H, CH_3), 3.81 (q, 2H, CH_2), 6.40 (s, 1H, CH thiazole), 7.43–8.56 (8H, m, Ar–H). ^{13}C NMR (DMSO-d6, δ, ppm): 13.45 (CH_2–CH_3), 14.11 (CH_3), 39.59 (CH_2–CH_3), 109.34, 121.08, 125.23, 129.14, 129.18, 132.06, 136.07, 144.70, 149.43, 153.96, 157.79 (ArC), 164.91 (C=N), MS *m*/*z* (RA%): 322 (M^+) (34%).

*(E)-4-(4-Bromophenyl)-3-ethyl-2-(((E)-1-(pyridin-2-yl)ethylidene) hydrazono)-2,3-dihydrothiazole (**5b**).* Yield 65%; mp (106–108) °C. Analysis for $C_{18}H_{17}BrN_4S$ (401.33) calcd: % C, 53.87; H, 4.27; N, 13.96; S, 7.99. Found: % C, 53.84; H, 4.27; N, 13.91; S, 7.93. IR (cm^{-1}, KBr): 1557 (C=N). ^1H NMR (DMSO-d6, δ, ppm): 1.14 (t, 3H, CH_3), 2.43 (s, 3H, CH_3), 3.81 (q, 2H, CH_2), 6.44 (s, 1H, CH thiazole), 7.43–8.61 (8H, m, Ar–H). ^{13}C NMR (DMSO-d6, δ, ppm): 13.43 (CH_2–CH_3), 14.12 (CH_3), 39.59 (CH_2–CH_3), 109.54, 121.28, 125.34, 129.45, 129.20, 131.56, 136.23, 144.34, 149.40, 154.06, 158.09 (Ar–C), 164.54 (C=N), MS *m*/*z* (RA%): 402 (M^+ + 1) (52%).

4.1.2. Synthesis of 2-(((*E*)-1-(pyridin-2-yl)ethylidene) hydrazono)thiazolidin-4-one derivatives (6–8). Compounds **1a** and **1b** (10 mmol) were refluxed for eight hours along with anhydrous sodium acetate (25 mmol), ethyl 2-bromopropionate, ethyl 2-chloroacetoacetate, or ethyl bromoacetate (10 mmol), and 100% ethanol (20 mL). After cooling, the precipitate that had formed was filtered out, repeatedly cleaned with water, dried, and recrystallized from absolute ethanol to provide the respective compounds (**6–8**).

*(E)-3-Ethyl-2-(((E)-1-(pyridin-2-yl)ethylidene)hydrazono) thiazolidin-4-one (**6b**).* Yield 90%; mp (133–135) °C. Analysis for $C_{12}H_{14}N_4OS$ (262.089) calcd: % C, 54.94; H, 5.38; N, 21.36; S, 12.22. Found: % C, 54.85; H, 5.36; N, 21.32; S, 12.26. IR (cm^{-1}, KBr): 1715 (C=O), 1554 (C=N). ^1H NMR (DMSO-d6, δ, ppm): 1.19 (t, 3H, CH_3), 2.44 (s, 3H, CH_3), 3.77 (q, 2H, CH_2), 3.94 (S, 2H, CH_2 thiazole), 7.43 (H, t, Ar–H), 7.84 (H, t, Ar–H), 8.04 (H, d, Ar–H), 8.61 (H, d, Ar–H), ^{13}C NMR (DMSO-d6, δ, ppm): 12.85 (CH_2–CH_3), 14.13 (CH_3), 32.39 (CH_2 thiazole), 38.13 (CH_2–CH_3), 121.99, 136.57, 149.05, 155.95 (Ar–C), 158.23 (C4 thiazole), 164.46 (C=N), 170.64 (C=O), MS *m*/*z* (RA%): 262 (M^+) (13%).

*(E)-5-Methyl-2-(((E)-1-(pyridin-2-yl)ethylidene)hydrazono) thiazolidin-4-one (**7a**).* Yield 85%; mp (176–178) °C. Analysis for $C_{11}H_{12}N_4OS$ (248.30) calcd: % C, 53.21; H, 4.87; N, 22.56; S, 12.91. Found: % C, 53.24; H, 4.83; N, 22.51; S, 12.97. IR (cm^{-1}, KBr): 3375 (NH), 1712 (C=O), 1554 (C=N), ^1H NMR (DMSO-d6, δ, ppm): 1.47 (d, 3H, CH_3), 2.39 (s, 3H, CH_3), 4.13 (q, 2H, CH_2), 7.39 (H, t, Ar–H), 7.83 (H, t, Ar–H), 8.02 (H, d, Ar–H), 8.59 (H, d, Ar–H), 12.0 (1H, s, NH). ^{13}C NMR (DMSO-d6, δ, ppm): 14.07 (CH_3), 19.33 (CH_3), 42.67 (CH_2 thiazole), 120.91, 124.91, 137.02, 149.33, 154.61 (Ar–C), 155.76 (C1 thiazole), 161.71 (C=N), 177.56 (C=O), MS *m*/*z* (RA%): 248 (M^+) (10%).

*(E)-3-Ethyl-5-methyl-2-(((E)-1-(pyridin-2-yl)ethylidene) hydrazono)thiazolidin-4-one (**7b**).* Yield 80%; mp (95–97) °C.

Open Access Article. Published on 07 October 2024. Downloaded on 2/11/2026 10:58:08 AM. This article is licensed under a Creative Commons Attribution-NonCommercial 3.0 Unported Licence.

Analysis for $C_{13}H_{16}N_4OS$ (276.36) calcd: % C, 56.50; H, 5.84; N, 20.27; S, 11.60. Found: % C, 56.55; H, 5.80; N, 20.29; S, 11.65. IR (cm^{-1}, KBr): 1708 (C=O), 1561 (C=N), ^{1}H NMR (DMSO-d6, δ, ppm): 1.18 (t, 3H, CH_3), 1.49 (d, 3H, CH_3), 2.43 (s, 3H, CH_3), 3.76 (q, 2H, CH_2–CH_3), 4.22 (q, 2H, S–CH_2), 7.41 (H, t, Ar–H), 7.83 (H, t, Ar–H), 8.04 (H, d, Ar–H) 8.60 (H, d, Ar–H), ^{13}C NMR (DMSO-d6, δ, ppm): 12.78 (CH_2–CH_3), 14.07 (CH_3), 19.32 (CH_3), 38.59 (CH_2–CH_3), 41.90 (CH_2 thiazole), 120.97, 125.14, 137.13, 149.42, 155.57 (Ar–C), 157.13 (C1 thiazole), 162.58 (C=N), 176.23 (C=O) MS *m*/*z* (RA%): 276 (M^+) (12%).

*(E)-5-Acetyl-2-(((E)-1-(pyridin-2-yl)ethylidene)hydrazono) thiazolidin-4-one (**8a**).* Yield 75%; mp (118–120) °C. Analysis for $C_{12}H_{12}N_4O_2S$ (276.31) calcd: % C, 56.16; H, 4.38; N, 20.28; S, 11.60. Found: % C, 56.18; H, 4.34; N, 20.18; S, 11.65. IR (cm^{-1}, KBr): 3330 (NH), 1542 (C=N), 1995, 1703 (2C=O), ^{1}H NMR (DMSO-d6, δ, ppm): 2.40 (s, 3H, $COCH_3$), 2.47 (s, 3H, CH_3), 4.17 (s, 1H, CH thiazole), 7.43 (1H, t, Ar–H), 7.79 (1H, t, Ar–H), 8.06 (1H, d, Ar–H), 8.55 (1H, d, Ar–H), 11.92 (1H, s, NH). ^{13}C NMR (DMSO-d6, δ, ppm): 14.82 (CH_3), 22.52 ($COCH_3$), 61.06 (CH thiazole), 122.18, 126.77, 136.54, 149.27, 154.12, 158.80 (C1 thiazole), 164.53 (C=N), 170.95 (C=O), 197.98 ($COCH_3$), MS *m*/*z* (RA%): 276 (M^+) (0.75%).

*(E)-5-Acetyl-3-ethyl-2-(((E)-1-(pyridin-2-yl)ethylidene)hydrazono) thiazolidin-4-one (**8b**).* Yield 60%; mp (94–96) °C. Analysis for $C_{14}H_{16}N_4O_2S$ (304.37) calcd: % C, 55.25; H, 5.30; N, 18.41; S, 10.53. Found: % C, 55.28; H, 5.35; N, 18.46; S, 10.48. IR (cm^{-1}, KBr): 1543 (C=N), 1703 (2C=O), ^{1}H NMR (DMSO-d6, δ, ppm): 1.24 (3H, t, CH_3), 2.40 (s, 3H, $COCH_3$), 2.43 (s, 3H, CH_3), 3.98 (q, 2H, CH_2), 4.19 (s, 1H, CH thiazole), 7.34 (1H, t, Ar–H), 7.79 (1H, t, Ar–H), 8.08 (1H, d, Ar–H), 8.55 (1H, d, Ar–H). ^{13}C NMR (DMSO-d6, δ, ppm): 13.49 (CH_2–CH_3), 14.83 (CH_3), 22.52 ($COCH_3$), 35.72 (CH_2–CH_3), 61.09 (CH_2 thiazole), 122.18, 126.72, 136.54, 149.27, 154.12 (Ar–C), 158.80 (C1 thiazole), 164.53 (C=N), 170.80 (C=O), 197.38 ($COCH_3$). MS *m*/*z* (RA%): 304 (M^+) (0.98%).

4.1.3. Synthesis of (*E*)-5-((*E*)-benzylidene)-2-(((*E*)-1-(pyridin-2-yl)ethylidene)hydrazono)thiazolidin-4-one derivatives (9a,b–12a,b). (a) Compounds **1a** and **1b** (10 mmol) and ethyl bromoacetate (10 mmol) were combined with an equimolar amount of suitable aromatic aldehydes (5-flouro-benzaldehyde, 4-chloro-benzaldehyde, 4-methoxy benzaldehyde, and/or 3,4-dimethoxybenzaldehyde) (10 mmol) in 10 mL of acetic acid (10 mL) and 25 mmol of anhydrous sodium acetate (25 mmol) and refluxed for eight hours. The matching compounds were obtained by filtering off the precipitate, washing it with water, drying it, and recrystallizing it from absolute ethanol after it had cooled (**9a,b–12a,b**).

(b) In glacial acetic acid (10 mL) and anhydrous sodium acetate (25 mmol), a mixture of compounds **6a** and **6b** (10 mmol) with an equimolar amount of an appropriate aromatic aldehyde, namely, 4-fluoro-benzaldehyde, 4-chloro-benzaldehyde, 4-methoxy benzaldehyde and/or 3,4-dimethoxybenzaldehyde (10 mmol), was refluxed for 6–8 hours, cooled, and then placed into cold water. The resulting chemicals were obtained by collecting and crystallizing the solid that was generated from absolute ethanol (**9a,b–12a,b**).

*(E)-5-((E)-4-Fluorobenzylidene)-2-(((E)-1-(pyridin-2-yl) ethylidene)hydrazono)thiazolidin-4-one (**9a**).* Yield 75%; mp (204–206) °C. Analysis for $C_{17}H_{13}FN_4OS$ (340.38) calcd: % C, 59.99; H, 4.85; N, 16.46; S, 9.42. Found: % C, 59.94; H, 4.75; N, 16.41; S, 9.46. IR (cm^{-1}, KBr): 3325 (NH), 1692 (C=O), 1550 (2C=N). ^{1}H NMR (DMSO-d6, δ, ppm): 2.46 (s, 3H, CH_3), 7.18–8.63 (9H, m, Ar–H + CH benzylic), 12.16 (1H, s, NH). ^{13}C NMR (DMSO-d6, δ, ppm): 14.50 (CH_3), 115.52, 115.56, 124.10, 125.45, 131.10, 136.42, 142.91, 149.19, 154.13, 159.62, 162.14 (Ar–C + CH benzylic + C2, C5 thiazole), 164.53 (C=N), 164.34 (C=O), MS *m*/*z* (RA%): 340 (M^+) (5.78%).

*(E)-3-Ethyl-5-((E)-4-fluorobenzylidene)-2-(((E)-1-(pyridin-2-yl) ethylidene)hydrazono)thiazolidin-4-one (**9b**).* Yield 70%; mp (125–127) °C. Analysis for $C_{19}H_{17}FN_4OS$ (368.43) calcd: % C, 61.94; H, 4.65; N, 15.21; S, 8.70. Found: % C, 61.99; H, 4.60; N, 15.26; S, 8.67. IR (cm^{-1}, KBr): 1695 (C=O), 1554 (C=N). ^{1}H NMR (DMSO-d6, δ, ppm): 1.13 (t, 3H, CH_3), 2.47 (s, 3H, CH_3), 3.78 (q, 3H, CH_2), 7.72–8.51 (9H, m, Ar–H + CH benzylic). ^{13}C NMR (DMSO-d6, δ, ppm): 12.85 (CH_2–CH_3), 14.59 (CH_3), 35.58 (CH_2–CH_3), 115.52, 115.56, 124.10, 125.45, 131.10, 136.42, 142.91, 149.19, 154.13, 159.62, 162.14 (Ar–C + CH benzylic + C1, C5 thiazole), 164.53 (C=N), 164.34 (C=O), MS *m*/*z* (RA%): 368 (M^+) (0.78%).

*(E)-5-((E)-4-Chlorobenzylidene)-2-(((E)-1-(pyridin-2-yl) ethylidene)hydrazono)thiazolidin-4-one (**10a**).* Yield 65%; mp (119–121) °C. Analysis for $C_{17}H_{13}ClN_4OS$ (356.83) calcd: % C, 57.22; H, 3.67; N, 15.70; S, 8.98. Found: % C, 57.28; H, 3.69; N, 15.10; S, 8.94. IR (cm^{-1}, KBr): 3326 (NH), 1696 (C=O), 1552 (C=N). ^{1}H NMR (DMSO-d6, δ, ppm): 2.47 (s, 3H, CH_3), 7.46–8.51 (9H, m, Ar–H + CH benzylic), 11.67 (1H, s, NH). ^{13}C NMR (DMSO-d6, δ, ppm): 14.55 (CH_3), 116.33, 120.90, 126.20, 127.55, 129.99, 133.10, 135.74, 143.72, 149.72, 154.13, 158.07 (Ar–C + CH benzylic + C1, C5 thiazole), 164.40 (C=N), 172.02 (C=O), MS *m*/*z* (RA%): 356 (M^+) (2.89%).

*(E)-5-((E)-4-Chlorobenzylidene)-3-ethyl-2-(((E)-1-(pyridin-2-yl) ethylidene)hydrazono)thiazolidin-4-one (**10b**).* Yield 80%; mp (146–148) °C. Analysis for $C_{19}H_{17}ClN_4OS$ (384.88) calcd: % C, 59.29; H, 4.45; N, 14.56; S, 8.33. Found: % C, 59.19; H, 4.49; N, 14.52; S, 8.38. IR (cm^{-1}, KBr): 1698 (C=O), 1556 (C=N). ^{1}H NMR (DMSO-d6, δ, ppm): 1.13 (t, 3H, CH_3), 2.47 (s, 3H, CH_3), 3.70 (q, 3H, CH_2), 7.47–8.51 (8H, m, Ar–H + CH benzylic). ^{13}C NMR (DMSO-d6, δ, ppm): 12.42 (CH_2–CH_3), 14.66 (CH_3), 35.63 (CH_2–CH_3), 116.62, 120.90, 126.26, 127.99, 129.99, 133.83, 135.74, 143.79, 149.62, 154.18, 158.12 (Ar–C + CH benzylic + C2, C5 thiazole), 164.77 (C=N), 166.32 (C=O), MS *m*/*z* (RA%): 384 (M^+) (20%).

*(E)-5-((E)-4-Methoxybenzylidene)-2-(((E)-1-(pyridin-2-yl) ethylidene)hydrazono)thiazolidin-4-one (**11a**).* Yield 50%; mp (155–157) °C. Analysis for $C_{18}H_{16}N_4O_2S$ (352.41) calcd: % C, 61.35; H, 4.58; N, 15.90; S, 9.10. Found: % C, 61.29; H, 4.52; N, 15.98; S, 9.14. IR (cm^{-1}, KBr): 3328 (NH), 1694 (C=O), 1552 (C=N). ^{1}H NMR (DMSO-d6, δ, ppm): 2.47 (s, 3H, CH_3), 3.73 (s, 3H, OCH_3), 6.99–8.44 (9H, m, Ar–H + CH benzylic), 11.62 (1H, s, NH). ^{13}C NMR (DMSO-d6, δ, ppm): 14.54 (CH_3), 56.65 (OCH_3), 114.54, 116.62, 122.76, 126.26, 127.64, 130.64, 137.36, 143.72, 148.70, 154.13, 156.80 (Ar–C + CH benzylic + C2, C5 thiazole), 164.40 (C=N), 174.53 (C=O), MS *m*/*z* (RA%): 352 (M^+) (24.14%).

*(E)-3-Ethyl-5-((E)-4-methoxybenzylidene)-2-(((E)-1-(pyridin-2-yl) ethylidene)hydrazono)thiazolidin-4-one (**11b**).* Yield 75%; mp (150–152) °C. Analysis for $C_{20}H_{20}N_4O_2S$ (380.47) calcd: % C,

 © 2024 The Author(s). Published by the Royal Society of Chemistry

Open Access Article. Published on 07 October 2024. Downloaded on 2/11/2026 10:58:08 AM. This article is licensed under a Creative Commons Attribution-NonCommercial 3.0 Unported Licence.

63.14; H, 5.30; N, 14.73; S, 8.43. Found: % C, 63.19; H, 5.37; N, 14.70; S, 8.47. IR (cm^{-1}, KBr): 1699 (C=O), 1554 (C=N). ^{1}H NMR (DMSO-d6, δ, ppm): 1.14 (t, 3H, CH_3), 2.47 (s, 3H, CH_3), 3.69 (s, 3H, OCH_3), 3.71 (q, 2H, CH_2), 6.99–8.44 (9H, m, Ar–H + CH benzylic), ^{13}C NMR (DMSO-d6, δ, ppm): 12.96 (CH_2–CH_3), 14.66 (CH_3), 35.63 (CH_2–CH_3), 56.61 (OCH_3), 114.54, 116.75, 122.92, 126.26, 127.99, 130.55, 137.29, 143.27, 148.65, 154.18, 156.80 (Ar–C + CH benzylic + C2, C5 thiazole), 164.36 (C=N), 166.55 (C=O), MS *m*/*z* (RA%): 380 (M^+) (1.31%).

*(E)-5-((E)-3,4-Dimethoxybenzylidene)-2-(((E)-1-(pyridin-2-yl) ethylidene)hydrazono)thiazolidin-4-one (**12a**).* Yield 70%; mp (143–145) °C. Analysis for $C_{19}H_{18}N_4O_3S$ (382.44) calcd: % C, 59.67; H, 4.74; N, 14.65; S, 8.38. Found: % C, 59.71; H, 4.64; N, 14.60; S, 8.32. IR (cm^{-1}, KBr): 3329 (NH), 1696 (C=O), 1554 (C=N). ^{1}H NMR (DMSO-d6, δ, ppm): 2.47 (s, 3H, CH_3), 3.78, 3.81 (s, 6H, 2OCH_3), 7.01–8.44 (9H, m, Ar–H + CH benzylic), 11.90 (s, 1H, NH), ^{13}C NMR (DMSO-d6, δ, ppm): 14.59 (CH_3), 56.69 (OCH_3), 110.97, 111.01, 116.62, 120.14, 122.93, 122.97, 126.20, 136.27, 143.68, 149.40, 149.24, 154.24, 158.07 (Ar–C + CH benzylic + C2, C5 thiazole), 164.62 (C=N), 174.46 (C=O), MS *m*/*z* (RA%): 382 (M^+) (5.14%).

*(E)-5-((E)-3,4-Dimethoxybenzylidene)-3-ethyl-2-(((E)-1-(pyridin-2-yl)ethylidene)hydrazono)thiazolidin-4-one (**12b**).* Yield 65%; mp (173–175) °C. Analysis for $C_{21}H_{22}N_4O_3S$ (410.141) calcd: % C, 61.45; H, 5.40; N, 13.65; S, 7.81. Found: % C, 61.49; H, 5.30; N, 13.62; S, 7.87. IR (cm^{-1}, KBr): 1698 (C=O), 1559 (C=N). ^{1}H NMR (DMSO-d6, δ, ppm): 1.16 (t, 3H, CH_3), 2.47 (s, 3H, CH_3), 3.71, 3.72 (2s, 6H, 2OCH_3), 3.74 (q, 2H, CH_2), 6.99–8.44 (9H, m, Ar–H + CH benzylic), ^{13}C NMR (DMSO-d6, δ, ppm): 12.85 (CH_2–CH_3), 14.55 (CH_3), 35.63 (CH_2–CH_3), 56.68 (OCH_3), 115.47, 116.54, 122.93, 127.99, 129.99, 138.57, 143.27, 148.70, 154.84, 156.12, (Ar–C + CH benzylic + C2, C5 thiazole), 164.62 (C=N), 166.06 (C=O), MS *m*/*z* (RA%): 410 (M^+) (0.34%).

4.1.4. Synthesis of (*E*)-5-((*E*)-phenyldiazenyl)-2-(((*E*)-1-(pyridin-2-yl)ethylidene)hydrazono)-2,3-dihydrothiazole derivatives (13a,b & 14a,b). Compounds **1a** and **1b** (10 mmol) were combined with suitable hydrazonoyl chlorides (10 mmol) in 30 mL of absolute ethanol that included 10 mmol of triethylamine. The mixture was refluxed for 10 hours before being cooled. To get compounds **13a,b** & **14a,b**, the precipitate that had formed was filtered out, cleaned with ethanol, dried, and recrystallized from absolute ethanol.

*(E)-4-Methyl-2-(((E)-1-(pyridin-2-yl)ethylidene)hydrazono)-5-((E)-p-tolyldiazenyl)-2,3-dihydrothiazole (**13a**).* Yield 60%; mp (150–152) °C. Analysis for $C_{18}H_{18}N_6S$ (350.44) calcd: % C, 61.69; H, 5.18; N, 23.98; S, 9.15. Found: % C, 61.60; H, 5.28; N, 23.93; S, 9.18. IR (cm^{-1}, KBr): 3310 (NH); 1550 (C=N). ^{1}H NMR (DMSO-d6, δ, ppm): 2.44 (s, 3H, CH_3), 2.45 (s, 3H, CH_3), 2.47 (s, 3H, CH_3), 7.37–8.59 (8H, m, Ar–H), 10.65 (1H, s, NH). ^{13}C NMR (DMSO-d6, δ, ppm): 12.17 (CH_3), 14.99 (CH_3), 21.76 (CH_3), 94.02 (C5 thiazole), 122.93, 126.08, 129.01, 129.38, 136.46, 137.80, 144.41, 149.66, 153.73, 154.18, 158.67 (Ar–C + C2, C4 thiazole), 165.28 (C=N), MS *m*/*z* (RA%): 350 (M^+) (37%).

*(E)-3-Ethyl-4-methyl-2-(((E)-1-(pyridin-2-yl)ethylidene)hydrazono)-5-((E)-p-tolyldiazenyl)-2,3-dihydrothiazole (**13b**).* Yield 65%; mp (148–150) °C. Analysis for $C_{20}H_{22}N_6S$ (378.50) calcd: % C, 63.47; H, 5.86; N, 22.20; S, 8.47. Found: % C, 63.41; H, 5.80; N, 22.27; S, 8.37, IR (cm^{-1}, KBr): 1552 (C=N). ^{1}H NMR (DMSO-d6, δ, ppm): 1.34 (t, 3H, CH_3), 2.43 (s, 3H, CH_3), 2.45 (s, 3H, CH_3), 2.47 (s, 3H, CH_3), 4.12 (q, 2H, CH_2), 7.46–8.60 (8H, m, Ar–H). ^{13}C NMR (DMSO-d6, δ, ppm): 10.15 (CH_3), 12.58 (CH_3), 14.59 (CH_3), 21.62 (CH_3), 42.35 (CH_2–CH_3), 93.69 (C5 thiazole), 122.88, 126.08, 129.06, 129.89, 136.51, 138.42, 144.41, 153.73, 155.07, 158.71 (Ar–C + C2, C4 thiazole), 164.41 (C=N). MS *m*/*z* (RA%): 378 (M^+) (49%).

*(E)-5-((E)-(4-Chlorophenyl)diazenyl)-3-ethyl-4-methyl-2-(((E)-1-(pyridin-2-yl)ethylidene)hydrazono)-2,3-dihydrothiazole (**14b**).* Yield 60%; mp (150–152) °C. Analysis for $C_{19}H_{19}ClN_6S$ (398.91) calcd: % C, 57.21; H, 4.80; N, 21.07; S, 8.04. Found: % C, 57.28; H, 4.85; N, 21.12; S, 8.08, IR (cm^{-1}, KBr): 1553 (C=N). ^{1}H NMR (DMSO-d6, δ, ppm): 1.34 (t, 3H, CH_3), 2.45 (s, 3H, CH_3), 2.47 (s, 3H, CH_3), 4.13 (q, 2H, CH_2), 7.37–8.63 (8H, m, Ar–H). ^{13}C NMR (DMSO-d6, δ, ppm): 10.03 (CH_3), 13.30 (CH_3), 14.56 (CH_3), 42.89 (CH_2–CH_3), 93.71 (C5 thiazole), 122.94, 126.26, 129.43, 129.99, 136.22, 138.30, 145.76, 149.54, 153.73, 154.18, 158.16 (Ar–C + C2, C4 thiazole), 164.32 (C=N), MS *m*/*z* (RA%): 398 (M^+) (47%).

4.2. Biological evaluation

4.2.1. *In vitro* anti-proliferative assay. The human cancer cell lines were brought from the American Type Culture Collection (ATCC; Washington, DC, USA) and were maintained as monolayer cultures in RPMI-1640 at the National Cancer Institute. The anti-proliferative activity was evaluated using the sulforhodamine-B (SRB) method following a previously reported method[70] and is explained in detail in the ESI.†

4.2.2. *In vitro* enzymatic inhibitory evaluation against CDK2 and GSK3β. Three promising hybrids **1a**, **8a** and **13a** were selected for enzymatic assay. The CDK2 assay kit and GSK3β assay kit were purchased from Bioscience Company and were used according to previously reported methods[53,54] and a detailed explanation is given in the ESI.†

4.2.3. Cell cycle analysis and detection of apoptosis. The cell cycle analysis and induction of apoptosis for the promising hybrid **13a** were assessed using flow cytometry.[55] HepG2 cells were incubated at 37 °C and treated with **13a** for 24 h. Further details are given in the ESI.†

4.2.4. The effect of compound 13a on the levels of Bax, Bcl-2 and caspase-3 in HepG2 cells. The effect of compound **13a** on apoptosis biomarkers in HepG2 was determined according to reported methods, and an extra explanation is given in the ESI.†

Data availability

The data supporting this article have been included as part of the ESI† associated with this article and can be found in the online version.

Author contributions

Asmaa F. Kassem: conceptualization, methodology, validation, formal analysis, investigation, resources, data curation, writing – original draft, writing – review & editing. Ashraf A. Sediek: conceptualization, methodology, validation, formal analysis,

Open Access Article. Published on 07 October 2024. Downloaded on 2/11/2026 10:58:08 AM. This article is licensed under a Creative Commons Attribution-NonCommercial 3.0 Unported Licence.

investigation, resources, data curation. Mervat M. Omran: software, investigation, data curation, writing – original draft. Doaa S. Foda: software, investigation, data curation, writing – review & editing. Aisha A. K. Al-Ashmawy: conceptualization, methodology, validation, formal analysis, investigation, resources, software, data curation, writing – original draft, writing – review & editing. All persons who meet authorship criteria are listed as authors, and all authors certify that they have participated sufficiently in the work to take public responsibility for the content, including participation in the concept, design, analysis, writing, or revision of the manuscript. All authors have read and agreed to the published version of the manuscript.

Conflicts of interest

There is no conflict to declare.

Acknowledgements

The authors thank the National Cancer Institute and National Research Centre for the equipment and facilities.

References

1 Y. Chen, X. F. Zhang and L. Ou-Yang, *Comput. Struct. Biotechnol. J.*, 2023, **21**, 974–990.
2 World Health Organization International Agency for Research on Cancer (IARC), *World Cancer Report: Cancer Research for Cancer Prevention*, 2020, vol. 199.
3 R. V. J. Chari, *Acc. Chem. Res.*, 2008, **41**, 98–107.
4 M. Brindisi, S. M. Kessler, V. Kumar and C. Zwergel, *Front. Oncol.*, 2022, **12**, 980141.
5 K. S. Bhullar, N. O. Lagarón, E. M. McGowan, I. Parmar, A. Jha, B. P. Hubbard and H. P. V. Rupasinghe, *Mol. Cancer*, 2018, **17**, 48.
6 G. Manning, D. B. Whyte, R. Martinez, T. Hunter and S. Sudarsanam, *Science*, 2002, **298**, 1912–1934.
7 J. Zhang, P. L. Yang and N. S. Gray, *Nat. Rev. Cancer*, 2009, **9**, 28–39.
8 A. A. K. Al-Ashmawy, K. M. Elokely, O. Perez-Leal, M. Rico, J. Gordon, G. Mateo, A. M. Omar, M. Abou-Gharbia and W. E. Childers, *ACS Med. Chem. Lett.*, 2020, **11**, 2156–2164.
9 A. A. K. Al-Ashmawy, F. A. Ragab, K. M. Elokely, M. M. Anwar, O. Perez-Leal, M. C. Rico, J. Gordon, E. Bichenkov, G. Mateo, E. M. M. Kassem, G. H. Hegazy, M. Abou-Gharbia and W. Childers, *Bioorg. Med. Chem. Lett.*, 2017, **27**, 3117–3122.
10 M. Malumbres, *Physiol. Rev.*, 2011, **91**, 973–1007.
11 S. Tadesse, A. T. Anshabo, N. Portman, E. Lim, W. Tilley, C. E. Caldon and S. Wang, *Drug Discovery Today*, 2020, **25**, 406–413.
12 T. Chohan, H. Qian, Y. Pan and J.-Z. Chen, *Curr. Med. Chem.*, 2014, **22**, 237–263.
13 T. A. Chohan, A. Qayyum, K. Rehman, M. Tariq and M. S. H. Akash, *Biomed. Pharmacother.*, 2018, **107**, 1326–1341.
14 O. A. E. F. M. Fathalla, M. A. H. Ismail, M. M. Anwar, K. A. M. Abouzid and A. A. K. Ramadan, *Med. Chem. Res.*, 2013, **22**, 659–673.
15 S. M. A. Ruiz and H. Eldar-Finkelman, *Front. Mol. Neurosci.*, 2022, **14**, 22.
16 B. W. Doble and J. R. Woodgett, *J. Cell Sci.*, 2003, **116**, 1175–1186.
17 K. D. Miller, M. Fidler-Benaoudia, T. H. Keegan, H. S. Hipp, A. Jemal and R. L. Siegel, *Cancer statistics for adolescents and young adults*, Wiley Online Libr., 2020, vol. 70, pp. 443–459.
18 T. Domoto, M. Uehara, D. Bolidong and T. Minamoto, *Cells*, 2020, **9**, 1–31.
19 J. A. Mccubrey, L. S. Steelman, F. E. Bertrand, N. M. Davis, M. Sokolosky, S. L. Abrams, G. Montalto, A. B. D'Assoro, M. Libra, F. Nicoletti, R. Maestro, J. Basecke, D. Rakus, A. Gizak, Z. Demidenko, L. Cocco, A. M. Martelli and M. Cervello, *Oncotarget*, 2014, **5**, 2881–2911.
20 M. Brindisi, S. M. Kessler, V. Kumar and C. Zwergel, *Front. Oncol.*, 2022, **12**, 985363.
21 A. M. Alqahtani and A. A. Bayazeed, *Arabian J. Chem.*, 2021, **14**(1), 102914.
22 Z. Lv, C. Sheng, T. Wang, Y. Zhang, J. Liu, J. Feng, H. Sun, H. Zhong, C. Niu and K. Li, *J. Med. Chem.*, 2010, **53**, 660–668.
23 M. Ravinder, B. Mahendar, S. Mattapally, K. V. Hamsini, T. N. Reddy, C. Rohit, K. Srinivas, S. K. Banerjee and V. J. Rao, *Bioorg. Med. Chem. Lett.*, 2012, **22**, 6010–6015.
24 M. M. Ghorab, F. A. Ragab, H. I. Heiba, M. S. A. Elsayed and W. M. Ghorab, *Bioorg. Chem.*, 2018, **80**, 276–287.
25 A. F. Kassem, M. A. Omar, E. S. Nossier, H. M. Awad and W. A. El-Sayed, *J. Mol. Struct.*, 2023, **1294**, 136358.
26 C. Li, S. Zhang, Y. Lu, Y. Zhang, E. Wang and Z. Cui, *PLoS One*, 2013, **8**(12), e84659.
27 A. Kazi, S. Xiang, H. Yang, D. Delitto, J. Trevino, R. H. Y. Jiang, M. Ayaz, H. R. Lawrence, P. Kennedy and S. M. Sebti, *Nat. Commun.*, 2018, **9**(1), 5154.
28 Y. Xu, D. Cheng, L. Hu, X. Dong, L. Lv, C. Zhang and J. Zhou, *Biocell*, 2023, **47**, 825–836.
29 B. S. Choudhary, Sukanya, P. Mehta, S. Bach, S. Ruchaud, T. Robert, B. Josselin, S. Filipek and R. Malik, *Bioorg. Med. Chem. Lett.*, 2021, **52**, 128375.
30 A. F. Kassem, M. A. Omar, E. S. Nossier, H. M. Awad and W. A. El-Sayed, *J. Mol. Struct.*, 2023, **1294**, 136358.
31 P. Makam, R. Kankanala, A. Prakash and T. Kannan, *Eur. J. Med. Chem.*, 2013, **69**, 564–576.
32 S. Carradori, B. Bizzarri, M. D'Ascenzio, C. De Monte, R. Grande, D. Rivanera, A. Zicari, E. Mari, M. Sabatino, A. Patsilinakos, R. Ragno and D. Secci, *Eur. J. Med. Chem.*, 2017, **140**, 274–292.
33 H. A. Ghabbour, A. A. Kadi, K. E. H. Eltahir, R. F. Angawi and H. I. El-Subbagh, *Med. Chem. Res.*, 2015, **24**, 3194–3211.
34 C. Tratrat, M. Haroun, E. Tsolaki, A. Petrou, A. Gavalas and A. Geronikaki, *Curr. Top. Med. Chem.*, 2020, **21**, 257–268.
35 A. Conroy, D. E. Stockett, D. Walker, M. R. Arkin, U. Hoch, J. A. Fox and R. E. Hawtin, *Cancer Chemother. Pharmacol.*, 2009, **64**, 723–732.
36 A. M. Shawky, M. A. S. Abourehab, A. N. Abdalla and A. M. Gouda, *Eur. J. Med. Chem.*, 2020, **185**(1), 111780.

 © 2024 The Author(s). Published by the Royal Society of Chemistry

Open Access Article. Published on 07 October 2024. Downloaded on 2/11/2026 10:58:08 AM.
This article is licensed under a Creative Commons Attribution-NonCommercial 3.0 Unported Licence.

37 J. M. Domínguez, A. Fuertes, L. Orozco, M. Del Monte-Millán, E. Delgado and M. Medina, *J. Biol. Chem.*, 2012, **287**, 893–904.
38 Y. Dong, L. Sui, Y. Tai, K. Sugimoto and M. Tokuda, *Anticancer Res.*, 2001, **21**, 103–108.
39 S. Shen, D. C. Dean, Z. Yu and Z. Duan, *Hepatol. Res.*, 2019, **49**, 1097–1108.
40 L. Ding, J. Cao, W. Lin, H. Chen, X. Xiong, H. Ao, M. Yu, J. Lin and Q. Cui, *Int. J. Mol. Sci.*, 2020, **21**, 1960.
41 C. Desbois-Mouthon, M.-J. Blivet-Van Eggelpoë, E. Beurel, M. Boissan, R. Delélo, A. Cadoret and J. Capeau, *Hepatology*, 2002, **36**, 1528–1536.
42 H. Goto, K. Kawano, I. Kobayashi, H. Sakai and S. Yanagisawa, *Oral Oncol.*, 2002, **38**, 549–556.
43 C. Xu, Z. Du, S. Ren and Y. Pian, *Ann. Clin. Lab. Sci.*, 2021, **51**, 285–294.
44 J. Qi, Y. Zheng, K. Qian, L. Tian, G. X. Zhang, Z. Cheng and Y. Wang, *J. Inorg. Biochem.*, 2017, **177**, 110–117.
45 N. S. M. Mokhtaruddin, E. N. M. Yusof, T. B. S. A. Ravoof, E. R. T. Tiekink, A. Veerakumarasivam and M. I. M. Tahir, *J. Mol. Struct.*, 2017, **1139**, 1–9.
46 F. Ali, K. M. Khan, U. Salar, M. Taha, N. H. Ismail, A. Wadood, M. Riaz and S. Perveen, *Eur. J. Med. Chem.*, 2017, **138**, 255–272.
47 M. D'Ascenzio, P. Chimenti, M. C. Gidaro, C. De Monte, D. De Vita, A. Granese, L. Scipione, R. Di Santo, G. Costa, S. Alcaro, M. Yáñez and S. Carradori, *J. Enzyme Inhib. Med. Chem.*, 2015, **30**, 908–919.
48 R. E. Khidre, S. R. El-Gogary and M. S. Mostafa, *J. Heterocycl. Chem.*, 2017, **54**, 2511–2519.
49 P. Skehan, R. Storeng, D. Scudiero, A. Monks, J. Mcmahon, D. Vistica, J. T. Warren, H. Bokesch, S. Kenney and M. R. Boyd, *J. Natl. Cancer Inst.*, 1990, **82**, 1107–1112.
50 D. Baskić, I. Jovanović, P. Ristić, V. Jakovljević, D. Delibašić and N. Arsenijević, in *Nitric Oxide*, 2005, vol. 6, pp. 49–52.
51 G. L. Ellman, *Arch. Biochem. Biophys.*, 1959, **82**, 70–77.
52 M. M. Bradford, *Anal. Biochem.*, 1976, **72**, 248–254.
53 U. Asghar, A. K. Witkiewicz, N. C. Turner and E. S. Knudsen, *Nat. Rev. Drug Discovery*, 2015, **14**, 130–146.
54 J. A. Mccubrey, L. S. Steelman, F. E. Bertrand, N. M. Davis, M. Sokolosky, S. L. Abrams, G. Montalto, A. B. D'Assoro, M. Libra, F. Nicoletti, R. Maestro, J. Basecke, D. Rakus, A. Gizak, Z. Demidenko, L. Cocco, A. M. Martelli and M. Cervello, *Oncotarget*, 2014, **5**, 2881–2911.
55 M. B. Labib, J. N. Philoppes, P. F. Lamie and E. R. Ahmed, *Bioorg. Chem.*, 2018, **76**, 67–80.
56 R. Jan and G. e. S. Chaudhry, *Adv. Pharm. Bull.*, 2019, **9**, 205–218.
57 P. Hussar, *Encyclopedia*, 2022, **2**, 1624–1636.
58 H. Kalkavan and D. R. Green, *Cell Death Differ.*, 2018, **25**, 46–55.
59 S. Qian, Z. Wei, W. Yang, J. Huang, Y. Yang and J. Wang, *Front. Oncol.*, 2022, **12**, 985363.
60 E. Eskandari and C. J. Eaves, *J. Cell Biol.*, 2022, **221**, e202201159.
61 A. Daina, O. Michielin and V. Zoete, *Sci. Rep.*, 2017, **7**, 1–13.
62 C. A. Lipinski, F. Lombardo, B. W. Dominy and P. J. Feeney, *Adv. Drug Delivery Rev.*, 2012, **64**, 4–17.
63 J. Ali, P. Camilleri, M. B. Brown, A. J. Hutt and S. B. Kirton, *J. Chem. Inf. Model.*, 2012, **52**, 420–428.
64 A. Daina and V. Zoete, *ChemMedChem*, 2016, 1117–1121.
65 O. Trott and A. J. Olson, *J. Comput. Chem.*, 2010, **31**, 455–461.
66 N. M. Abdelazeem, W. M. Aboulthana, Z. A. Elshahid, M. El-Hussieny and A. A. K. Al-Ashmawy, *J. Mol. Struct.*, 2024, **1310**, 138224.
67 D. J. Wood, S. Korolchuk, N. J. Tatum, L. Z. Wang, J. A. Endicott, M. E. M. Noble and M. P. Martin, *Cell Chem. Biol.*, 2019, **26**, 121–130.
68 P. Sivaprakasam, X. Han, R. L. Civiello, S. Jacutin-Porte, K. Kish, M. Pokross, H. A. Lewis, N. Ahmed, N. Szapiel, J. A. Newitt, E. T. Baldwin, H. Xiao, C. M. Krause, H. Park, M. Nophsker, J. S. Lippy, C. R. Burton, D. R. Langley, J. E. Macor and G. M. Dubowchik, *Bioorg. Med. Chem. Lett.*, 2015, **25**, 1856–1863.
69 E. Krieger, K. Joo, J. Lee, J. Lee, S. Raman, J. Thompson, M. Tyka, D. Baker and K. Karplus, *Proteins*, 2009, **77**, 114–122.
70 V. Vichai and K. Kirtikara, *Nat. Protoc.*, 2006, **1**, 1112–1116.